Synthetic Storm Modeling for Millimeter Wave Band Mesh Networks

Bharatwajan Raman

B.E., Electronics and Communication Engineering,
Anna University, India, 2005

Submitted to the Department of Electrical Engineering and Computer Science and the Faculty of the Graduate School of the University of Kansas in partial fulfillment of the requirements for the degree of Master of Science

Thesis Committee:

Dr. James P.G. Sterbenz: Chair

Dr. Alexander M. Wyglinski: Co-Chair

Dr. Victor S. Frost

Date Defended

2008/06/11

The thesis committee for Bharatwajan Raman certifies
that this is the approved version of the following thesis:

Synthetic Storm Modeling for Millimeter Wave Band Mesh Networks

Committee:

_____

Chair

_____

Co-Chair

_____

_____

Date Approved

Abstract

In this thesis, a novel method of modeling the characteristics of a storm and its effects on a millimeter wave band (70 – 90 GHz) mesh network is presented. A storm system is generated using synthetic data; the movement of the system through a network is simulated and attenuation on individual links is calculated using existing models relating rain rate and attenuation. Finally, the collective effect of attenuated links on network performance is analyzed. This model is particularly useful in implementing predictive routing algorithms, as knowledge of weather phenomenon is usually available several minutes in advance, which has the potential to improve or eliminate losses due to routing reconvergence.

Contents

Acceptance Page **i**

Abstract **ii**

List of Figures **vi**

List of Tables **vii**

1 Introduction **1**

1.1 Weather Disruption in the Real World 3

1.2 Research Contributions 4

1.2.1 Synthetic Storm Modeling 4

1.2.2 Simulation Model 5

1.2.3 Link Modeling 7

1.3 Thesis Organization 7

2 Background and Related Work **8**

2.1 Background 8

2.1.1 Millimeter Wave Transmission Systems 9

2.1.2 Losses in MWB Propagation 13

2.2 Related Work 20

2.2.1 Modeling Attenuation due to Rain 20

2.2.2 Link Modeling 24

2.2.3 Storm Modeling 25

3 Synthetic Storm Modeling **27**

3.1 Geometric Modeling 28

3.1.1 Storm Geometry 28
3.1.2 Storm Movement 31
3.2 Link Attenuation 32
3.2.1 Calculation of Fraction of Links Affected 33
3.2.2 Attenuation on Affected Links 37

4 Mesh Network Simulation **41**
4.1 Simulation Model 41
4.1.1 Storm Structure 42
4.1.2 Storm Patterns 42
4.2 Network Simulation and Parameters 42
4.2.1 Network Topology and Characteristics 43
4.2.2 Traffic 43
4.2.3 Performance Evaluation 44
4.3 Results and Analysis 44
4.3.1 Case 1: Vertical Storm Pattern 44
4.3.2 Case 2: Diagonal Storm Pattern 48
4.3.3 Case 3: Diagonal Pattern with Larger Storm 50

5 Link Modeling **55**
5.1 Markov Process 56
5.2 Measurement Setup 57
5.3 Three-State Markov Model 59

6 Conclusions and Future Work **65**
6.1 Conclusions 66
6.2 Future Work 67

A ITU-R P.838-3 Coefficients **70**

References **72**

List of Figures

1.1 Absorption by atmospheric elements [1, 2] 2
1.2 Absorption by atmospheric elements [2] 3
1.3 Obtaining FER on each link from the storm model 6

2.1 Free space path loss vs. distance 13
2.2 Gaseous absorption curves [2, 3] 15
2.3 Frequency vs. attenuation 18
2.4 Rain rate vs. attenuation 19
2.5 Crane rain zones in the US [2] 21

3.1 Elliptical modeling of storm 29
3.2 Radar image with light and heavy rain zones 30
3.3 Elliptical modeling of radar images 31
3.4 Storm movement generated in an 8×8 mesh 32
3.5 Storm movement in an arbitrary mesh with 6 nodes 33
3.6 Link entirely encompassed by the cell 35
3.7 Fraction of the link affected by the cell 36
3.8 Link covered at one end by the cell 36
3.9 FER vs. rain rate for a 1 mile link at 73.5 GHz 39
3.10 FER vs. rain rate for a 5 mile link at 73.5 GHz 40

4.1 Case 1: Topology of the mesh used in simulations 43
4.2 Case 1: Storm moves along the edge of a network 45
4.3 Case 1: Packets lost across affected links 46
4.4 Case 1: Throughput of all received bits 48
4.5 Case 1: Throughput of all dropped bits 48
4.6 Case 2: Storm moves diagonally across the network 49

4.7 Case 2: Throughput of all received bits 51
4.8 Case 2: Throughput of all dropped bits 51
4.9 Case 3: Storm moves diagonally across the network 52
4.10 Case 3: Throughput of all received bits 54
4.11 Case 3: Throughput of all dropped bits 54

5.1 MWB test topology 57
5.2 Three-state Markov model of link states 59
5.3 Quantization of link performance to three levels 60

6.1 Measured FER vs. FER derived from ITU-R P. 838-3 68

List of Tables

2.1 Beamwidth at 1 km with 30 cm diameter antennas 10
2.2 Fresnel zone clearance 11
2.3 Attenuation at 99.99% availability for a 3 km link [4] 23

4.1 Case 1: Simulation information 47
4.2 Case 2: Simulation information 50
4.3 Case 3: Simulation information 53

5.1 24-hour state probabilities without FEC (Jun. 2007) 61
5.2 24-hour TPM without FEC (Jun. 2007) 61
5.3 State probabilities with FEC (Jul. 2007–Feb. 2008) 61
5.4 TPM with FEC (Jul. 2007–Feb. 2008) 62
5.5 State probabilities without FEC (Jul. 2007–Feb. 2008) 62
5.6 TPM without FEC (Jul. 2007 – Feb. 2008) 62

A.1 Coefficients for k_H 70
A.2 Coefficients for k_V 70
A.3 Coefficients for α_H 71
A.4 Coefficients for α_V 71

Chapter 1

Introduction

The advent of video sharing sites, IPTV (internet protocol television), mobile video applications, and ubiquitous, highly affordable devices has ushered in an era of millions of people using voice and data networks, fixed and mobile for new applications. This trend is not likely to slow in the near future, and requires increasing bandwidth. Optical fibers provide the necessary bandwidth, but, not all carriers have access to affordable use of cables, and expansion is frequently impractical because of issues such as deployment costs [5, 6] and governmental regulations. In the wireless domain, the spectrum that is used by current technologies has been allocated by the Federal Communications Commission (FCC) in the US, but none of these technologies provide bandwidth comparable to that of optical fibers. The unlicensed 60 GHz band has been in use for some time now, but suffers range limitations due to oxygen absorption and weather-related attenuation. The free space optical band (FSO) can support higher bandwidths but is heavily attenuated by fog, smog, and other atmospheric impairments. Figures 1.1 and 1.2 show absorption due to atmospheric elements.

A lot of interest has been shown in the spectrum ranging from 70–95 GHz,

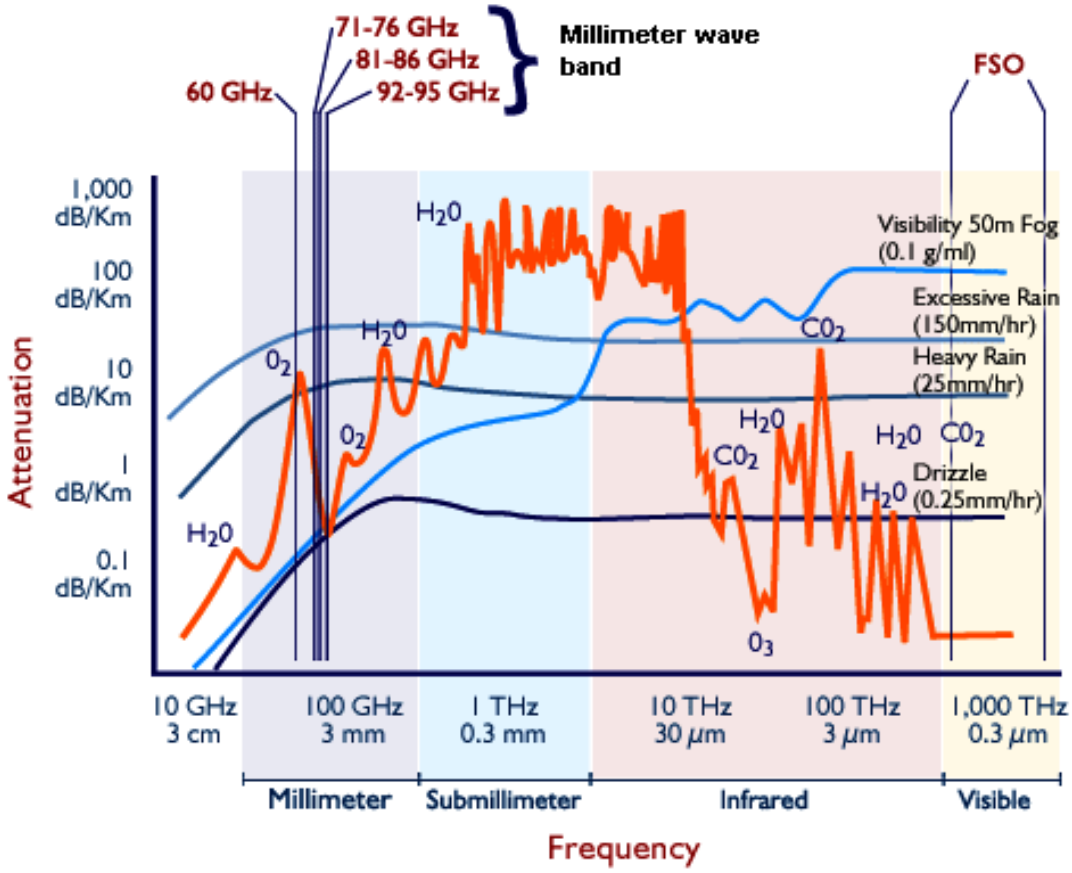

Figure 1.1. Absorption by atmospheric elements [1, 2]

referred to as millimeter wave band (MWB) after the FCC opened it for licensing. The MWB is particularly attractive for a variety of reasons such as high bandwidth, low interference, efficient frequency reuse, and light license regulations.

But, the paramount consideration in drafting link budgets at these frequencies is attenuation due to hydrometeors (rain, snow, hail, dew). There have been empirical models developed based on samples of rain measurements throughout the world that provide reasonable values of long-term fade probabilities, but they are highly specific to the area in which measurements were made and not useful to represent short-term channel conditions.

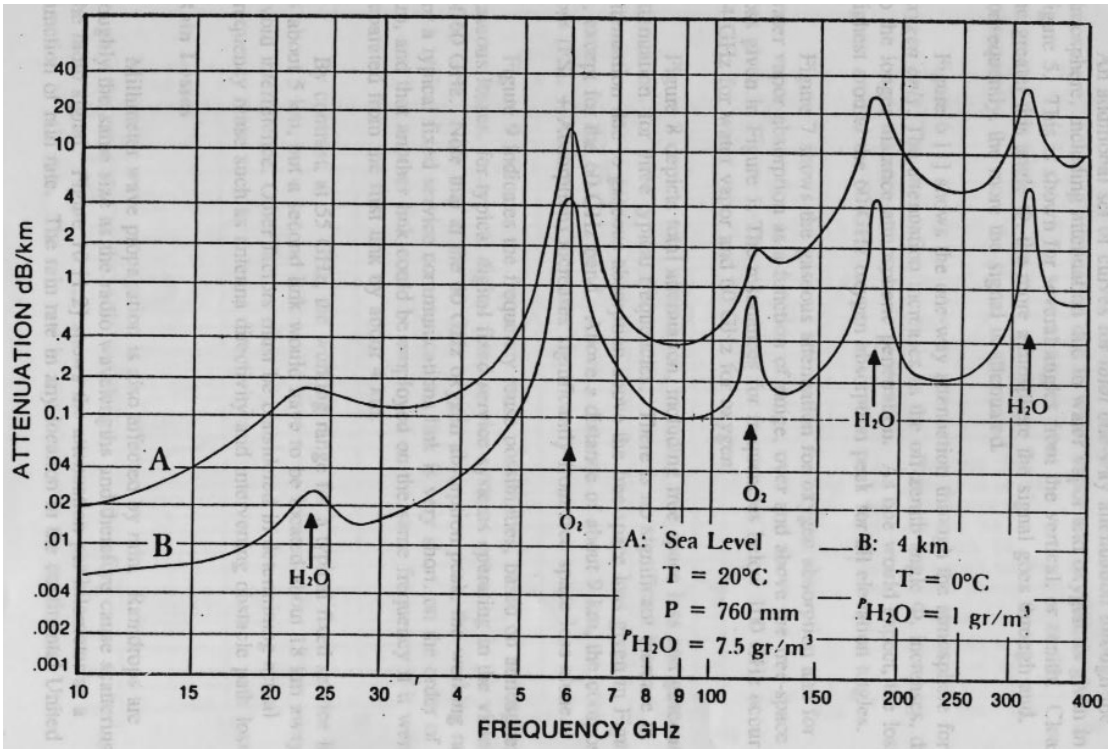

Figure 1.2. Absorption by atmospheric elements [2]

1.1 Weather Disruption in the Real World

In the real world, an assortment of atmospheric factors is responsible for signal degradation in MWB links with rain playing a major role. Higher values of rain rate result in greater attenuation.

For determining the performance of MWB mesh networks, it is important to understand the dynamics of weather phenomena and their effects on the links. This is not a straightforward task because the attenuation on a link is due to the collective effect of various factors such as rainfall rate, drop size, wind velocity, and polarization of the rain drops. Therefore, it is not easy to build an analytical model to capture weather effects on MWB transmissions. Furthermore, weather events are local in scope and bursty in nature; therefore deriving a generic analytical

expression to measure spatial correlation of rain attenuation is impractical. An impairment model is a more practical approach. While an empirical link model at best can capture rain attenuation along a single link, a simulation model is necessary to understand the effects of the weather event on the mesh network as a whole. This work proposes a technique to model effects of a storm system on a mesh network.

1.2 Research Contributions

The following are the major contributions of this thesis work:

- Develop a synthetic storm model with structure and trajectory which represents the characteristics of a real-world storm and model the effects of the storm on a millimeter wave mesh network.
- Simulate the effects of rain attenuation on network performance using the network simulator ns-2 [7].
- Formulate long-term statistics of rain attenuation using a three-state Markov model. The model is built from actual measurements of frame error rates on a physical link.

The following subsections introduce these contributions in more detail.

1.2.1 Synthetic Storm Modeling

A major portion of this work deals with modeling a storm system with multiple rain cells, simulating its movement through a mesh network, and calculating the attenuation on the links affected by the storm system passing above. The process

flow is detailed in Figure 1.3. This model can help simulate rain events and calculate attenuation due to rain on each link at every instant. If fed with real storm data, it can be used in real time to calculate and predict the attenuation on each link and hence will aid in developing predictive routing strategies to route around links affected by rain. The methodology is discussed in detail in Chapter 3.

1.2.2 Simulation Model

The effect of rain events on overall network performance is simulated using the ns-2 simulation package. A mesh-network model is built, CBR (constant bit rate) traffic is exchanged between arbitrary nodes, and loss on each link is modified according to the movement of the storm. Performance parameters such as throughput, delay, and number of packets dropped are monitored to evaluate mesh-network performance. The details of the simulation are discussed in Chapter 4.

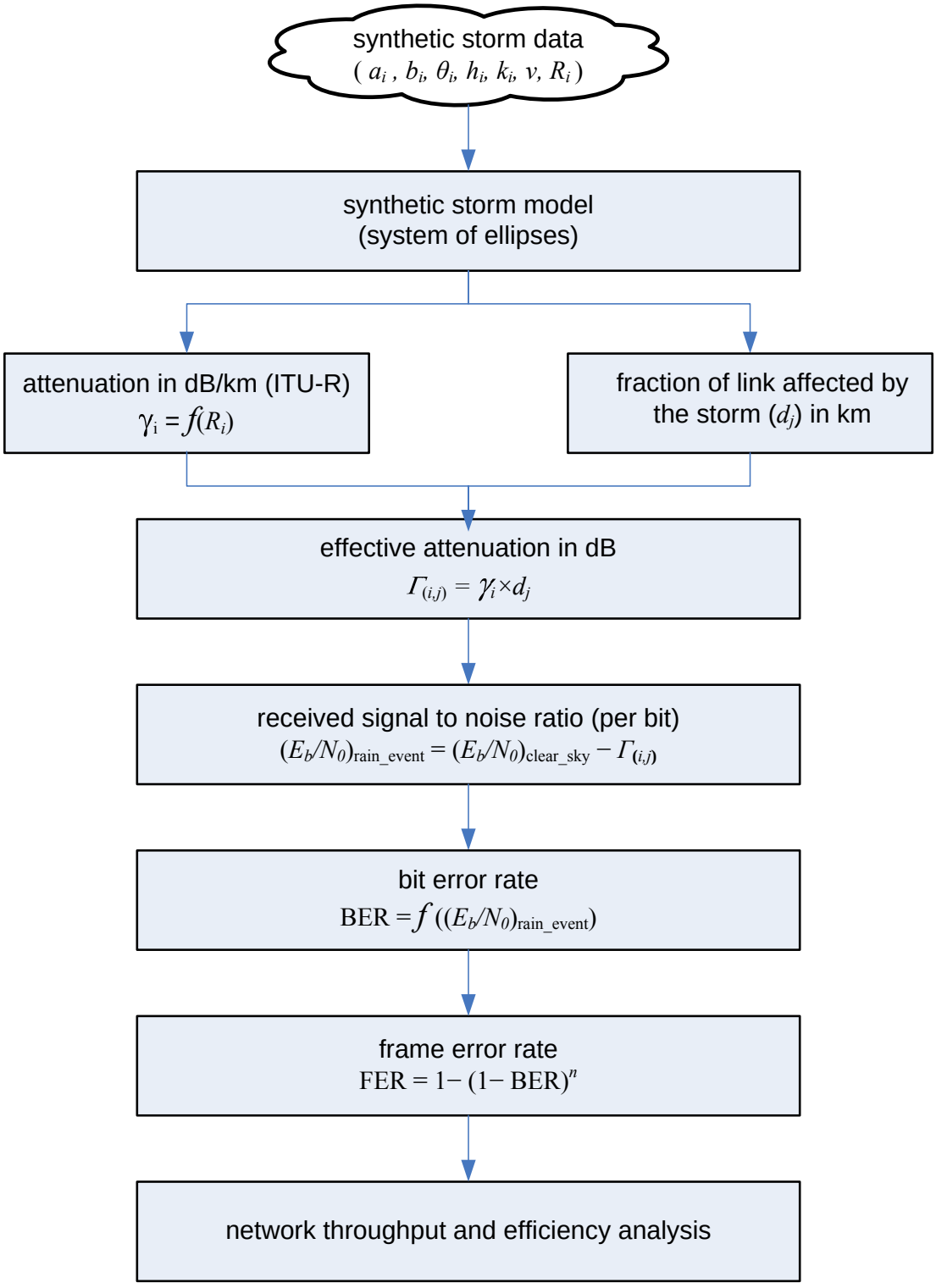

Figure 1.3. Obtaining FER on each link from the storm model

1.2.3 Link Modeling

A method to calculate long-term and short-term statistics of rain attenuation is also developed in this thesis. A Markov model representing strength of connectivity is constructed with three states: *strong*, *weak*, and *disconnected*. The model's state and state-transition probability values are obtained from measurements on a real link operating at 73.5 Ghz within the millimeter wave band. With this model, depending on the number of samples, we can obtain daily, monthly or yearly rain attenuation statistics. A useful quantity is worst-month statistics used by network planners to determine antenna gains on millimeter wave radios. The formulation of the model is explained in detail in Chapter 5.

1.3 Thesis Organization

The rest of the thesis is organized as follows: Chapter 2 discusses the properties of MWB signals and their propagation characteristics, losses suffered at MWB frequencies due to gaseous absorption, foliage, scattering and diffraction, and research work published in literature pertaining to rain attenuation modeling, link modeling, and storm modeling. Chapters 3, 4, and 5 detail the major contributions of this thesis. In Chapter 3, modeling of synthetic storms is presented. In Chapter 4, modeling of link behavior using a three-state Markov model is presented. In Chapter 5, mesh-network performance evaluation using ns-2 simulations is discussed. Chapter 6 outlines the conclusions arrived at from this research and future work that will improve this thesis and expand its scope.

Chapter 2

Background and Related Work

This chapter contains a background study on millimeter wave transmissions and a discussion of realted work in the areas of rain attenuation modeling, storm modeling, and link modeling.

This chapter is organized as follows: First, a background section details the properties of MWB (millimeter wave band) systems such as frequency bands, beamwidth, antenna, power requirements, and power spectral density and propagation characteristics such as losses and fading. Then, related work is presented that discusses works in literature that deal with rain attenuation and modeling storm systems.

2.1 Background

MWB communication technology is fairly new with the FCC inviting licensing bids as recently as 2003 in the US. Service rules for MWB were first specified in 2003 [8] and later modified in 2004 and 2005 [9]. This section details the characteristics of the MWB as well as losses in MWB links.

2.1.1 Millimeter Wave Transmission Systems

Transmission characteristics such as frequency range, beamwidth, antenna, power requirements, and power spectral density limits are discussed in this section. Knowledge of transmission characteristics is useful in designing nodes that are part of the mesh network used to simulate the effects of rain on network performance.

2.1.1.1 Frequency Band and Assignments

The range of frequencies between 30 GHz and 300 GHz have wavelengths on the order of millimeters. The MWB licensed by the FCC in the US consists of frequencies in the bands 71–76 GHz, 81–86 GHz and 92–95 GHz. The 92–95 GHz band is further divided into three segments: 92.0–94.0 GHz and 94.1–95.0 GHz for government and non government users and 94.0–94.1 GHz for US Federal Government use. Initially, the 71–76 GHz and 81–86 GHz bands were divided into four unpaired segments of 1.25 GHz each with a loading requirement of 1 bit/second/hertz (bps/Hz) with no aggregation limits. This was modified later to no segmentation and a loading requirement of 0.125 bps/Hz for ease of band reallocation and use of simple, inexpensive modulation schemes like on-off keying (OOK) or binary phase shift keying (BPSK) [9].

2.1.1.2 Beamwidth

Beamwidth is defined as the angle between the half-power points on the main lobe. The half-power, or the 3 dB points are with respect to the peak power of the main lobe. The beamwidth of a signal determines the density of the nodes in a network. Links operating with smaller beamwidths allow more spatial reuse permitting a greater number of nodes to be packed within a given geographi-

cal area compared to wider beamwidth links. Millimeter wave signals have very narrow beamwidth sometimes referred to as pencil beam. Table 2.1 shows the beamwidths of signals at different frequencies [10].

Table 2.1. Beamwidth at 1 km with 30 cm diameter antennas

Frequency [GHz]	**Beamwidth** [degrees]	**Beamwidth** [meters]
2.4	117°	1989
24	12°	204
60	4.7°	79.9
80	1.2°	20.4

It is seen that there is very little chance for interference if there is adequate seperation between antennas, which is in tens of meters as seen in Table 2.1. Higher diameter antennas reduce beamwidth, which enables a square mesh of several nodes with directional antennas in 4 orthogonal directions. Tests have indicated that it is possible to deploy up to 200 non interfering MWB antennas on the roof of a single skyscraper [9]. Fresnel zone calculations indicate a clearance of less than 10 meters from any obstruction needed for acceptable signal levels at the receiver. Fresnel zones are concentric regions in which the path length of the secondary waves differ by $n\lambda/2$ from that of the line of sight (LOS) component, where n is the n^{th} Fresnel zone and λ is the wavelength of the signal in meters [11]. A $\lambda/2$ difference in path length will cause a phase shift of 180°, thus causing destructive interference between the secondary wave and the LOS component. So, first Fresnel zone clearance is important to avoid interference. All components with a path length difference of odd multiples of $\lambda/2$ will cause destructive interference, but as n increases, the intensity of the secondary waves decreases. Table 2.2 shows a list of first Fresnel zone radii midway for antennas

seperated by distance d.

Table 2.2. Fresnel zone clearance

Frequency [GHz]	**First Fresnel zone** [m]	
	$d = 1$ km	$d = 5$ km
2.4	5.59	12.5
24	1.77	3.95
60	1.12	2.5
70	1.04	2.31
80	0.97	2.17

The Fresnel zone radius at any point P in the middle of a link is given by:

$$F_n = \sqrt{\frac{n\lambda d_1 d_2}{d_1 + d_2}} \tag{2.1}$$

where n is the n^{th} Fresnel zone, F_n is the radius of the n^{th} Fresnel zone in meters, d_1 is the distance of point P from one end of the link in km, d_2 is the distance of point P from the other end of the link in km, and λ is the wavelength of the signal in meters.

The first Fresnel zone contains the strongest signals. These numbers show that network planning will be relatively easy even in a dense urban environment. As beam spreading is minimal, structures and foliage will not cause interference if a line-of-sight path exists between the transmitter and receiver with a Fresnel first zone clearance from obstructing structures.

2.1.1.3 Antenna and Power Requirements

The FCC specifies a minimum antenna gain of 43 dBi (forward gain of the antenna compared to an isotropic antenna) and a half-power beamwidth of 1.2° for MWB links. Initial technical requirements specified a gain of 50 dBi and 0.6° half-power beamwidth. While larger beamwidths result in interference between closely spaced antennas, very small beamwidths have their own share of problems. A 0.6° half-power beamwidth and 50 dBi gain is possible only with two feet antennas which are more expensive than one-foot antennas that have a half-power beamwidth of 1.2°. In most places, existing infrastructure is insufficient to deploy bigger antennas; they need stronger towers thereby increasing deployment costs [9]. Finally, a 0.6° beamwidth signal complicates tower siting and often results in signal loss by the receiver because of tower sway, which is not uncommon in high-rise buildings. Error-angle fading (Section 2.1.2.5) is also pronounced at smaller beamwidths. The cost reduction by using smaller antennas enables wider deployment, thereby bridging the gap to buildings that are a couple of miles away from a fiber point-of-presence (POP) but that cannot have fiber connections [5,9].

2.1.1.4 Power Spectral Density Limit

Power spectral density (PSD) is a measure of how power is distributed across the frequencies in a particular frequency range. For example, given a range of 5 GHz and a transmit power limit of 7.5 W, it is possible to transmit the power using all of the 5 GHz bandwidth or only a portion of it, say, 100 MHz. The spectral properties of these two signals would be radically different. One of the main deployment advantages of MWB links is frequency reusability. This is made possible by the short range of wideband links. If no limit is imposed on power

spectral density, narrowband links can be used that will have a much longer range, thereby causing interference and reducing frequency reuse. Therefore, a PSD limit of 150 mW/100 MHz is enforced to make efficient use of the spectrum.

2.1.2 Losses in MWB Propagation

This section discusses losses due to various factors in MWB links. These losses consist of free space path loss, attenuation due to atmospheric gases, foliage loss, scattering and refractive effects in particulate matter, refractive effects and scintillation.

2.1.2.1 Free Space Path Loss

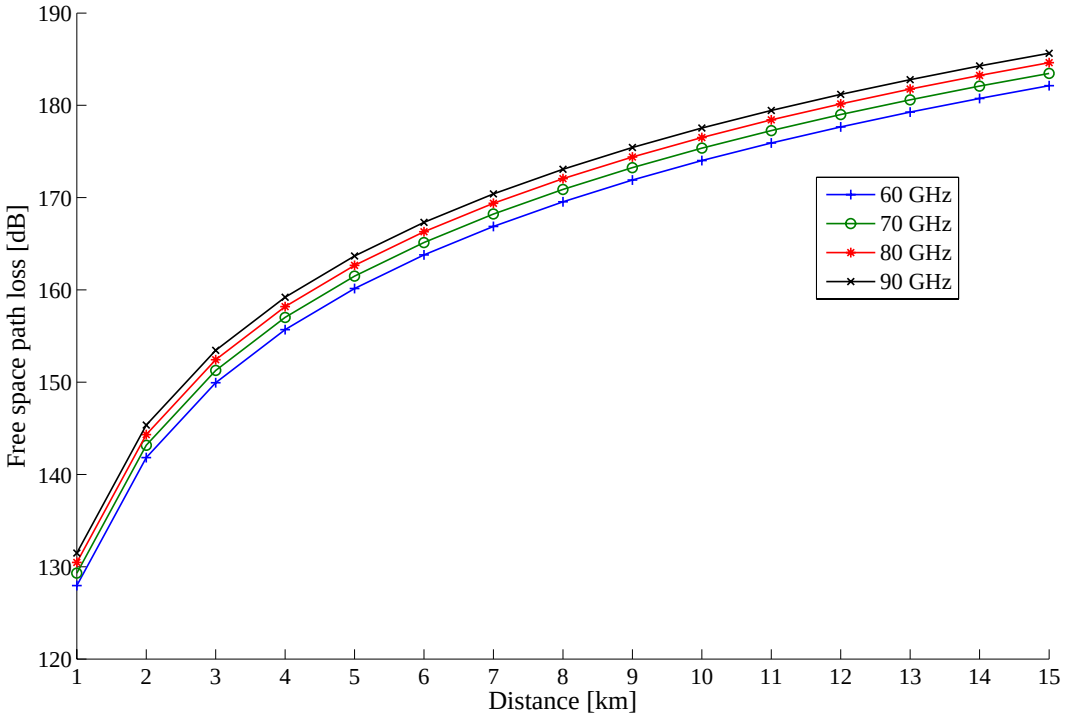

Figure 2.1. Free space path loss vs. distance

Free space path loss is the reduction in received signal strength with distance.

It is dependent on the frequency of the signal and the distance between the transmitting and receiving antennas.

In clear-sky conditions, free space path loss is given by [2]:

$$L_{\mathrm{FSL}} = (4\pi R/\lambda)^n \tag{2.2}$$

where, L_{FSL} is the free space path loss, R is the distance between transmit and receive antennas in km, λ is the operating wavelength in meters, and n is the path loss exponent. The path loss exponent is 2 in most cases.

Substituting $n = 2$ and rewriting in terms of frequency $[f]$,

$$L_{\mathrm{FSL}}\ [\mathrm{dB}] = 92.4 + 20\log f + 20\log R \tag{2.3}$$

Thus, the higher the frequency, the higher the path loss, for example, 129.5 dB for 71 GHz at 1 km and 131.2 GHz for 86 GHz at 1 km. Figure 2.1 shows free space path loss vs. distance for various millimeter wave frequencies, obtained from Equation 2.3. Given the fact that there are PSD limits and heavy path losses over larger distances, it is not possible to have very long millimeter wave links, and rain attenuation will further decrease the range of MWB links if availability requirements have to be met. Rain attenuation is discussed in Subsection 2.1.2.6.

2.1.2.2 Attenuation due to Atmospheric Gases

The major contributors to gaseous attenuation in MWB signals are oxygen and water vapor. Molecular interactions cause attenuation due to scattering and are appreciably higher near the frequency of resonance of the molecules. Attenuation

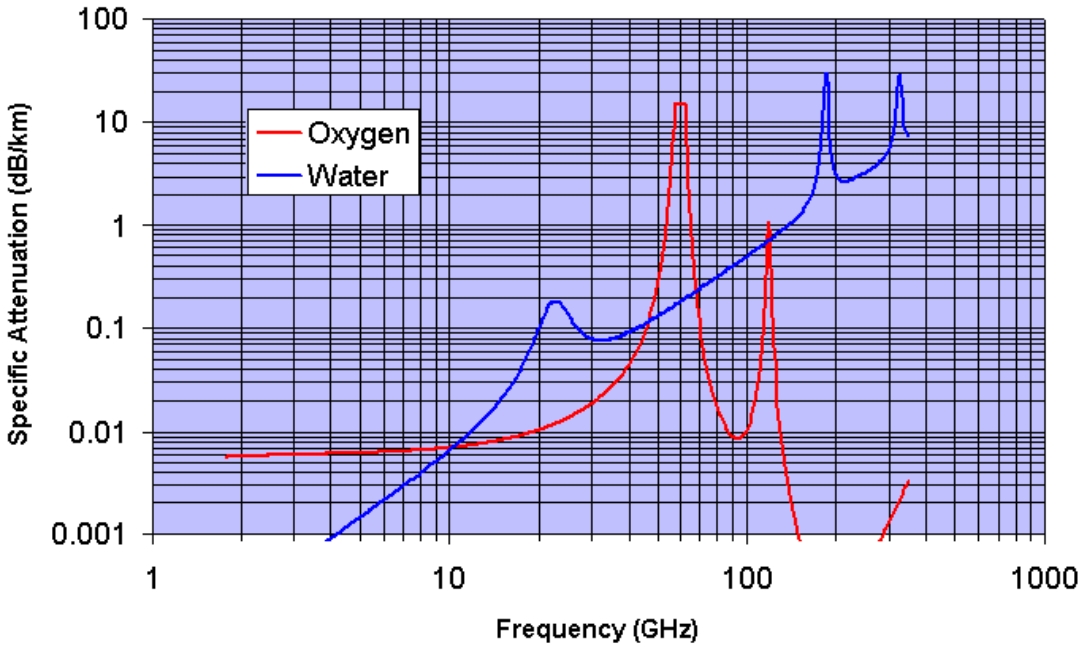

Figure 2.2. Gaseous absorption curves [2,3]

due to oxygen at ground level and a temperature of 15° is given by [12]:

$$\alpha_O[\text{dB/km}] = \left[3.79 \times 10^{-7} f + \frac{0.265}{(f-63)^2+1.59} + \frac{0.028}{(f-118)^2+1.47}\right](f+198)^2 \times 10^{-3} \tag{2.4}$$

for $f > 63$ GHz where f is the frequency of the signal.

Attenuation due to water vapor at sea level and at a temperature of 15° for $f < 350$ GHz and $\rho < 12$ g/m^3 where ρ is the water vapor density given by [12]:

$$\alpha_w[\text{dB/km}] = \left[0.050 + 0.0021\rho + \frac{3.6}{(f-22.2)^2+8.5} + \frac{10.6}{(f-183.3)^2+9} + \frac{8.9}{(f-325.4)^2+26.3}\right] f^2 \rho \times 10^{-4} \tag{2.5}$$

Note that these formulae are applicable at ground level within a pressure range of 1013 ± 50 mbar, at a temperature of 15°C. Other temperatures may be taken into account by correction factors of $-1\%^{\circ}\mathrm{C}^{-1}$ from 15°C for dry air, and $-0.6\%^{\circ}\mathrm{C}^{-1}$ from 15°C for water vapor, valid over the range from −20°C to +40°C. [13]

Figure 2.2 shows the losses due to oxygen and water vapor absorption. These plots were obtained from Equations 2.4 and 2.5, which are empirical formulae obtained from measurements.

2.1.2.3 Foliage Loss

The loss caused by vegetative obstructions is called foliage loss and it causes significant attenuation in millimeter wave frequencies. If there is foliage near the first Fresnel zone, multipath effects degrade the signal to a great extent. For a depth of less than 400 meters, the loss (L) is given by [2]:

$$L = 0.2 f^{0.3} R^{0.6} \tag{2.6}$$

where f is the frequency in MHz and R is the depth of foliage in meters (R <400). The above relationship is applicable for frequencies ranging between 0.2 GHz and 95 GHz.

2.1.2.4 Scattering and Absorption in Particulate Matter

Particulate matter such as sand and dust particles have sizes comparable to the wavelengths of millimeter wave signals. Hence, scattering is common when there is a lot of dust in the air. Other key properties apart from size that govern the extent of attenuation are shape, density, and dielectric properties of the particles.

The propagation constant a, is [14]

$$a = \alpha + j\beta \tag{2.7}$$

where,

$$\begin{aligned} \alpha &= 3.431 \times 10^6 f N r^3 \frac{\epsilon''}{(\epsilon'+2)^2 + \epsilon''^2} \\ \beta &= 7.545 \times 10^6 f N r^3 \frac{(\epsilon'-1)(\epsilon'+2) + \epsilon''^2}{(\epsilon'+2)^2 + \epsilon''^2} \end{aligned}$$

where, f is the frequency of the signal, N is the number of dust particles in unit volume, r is the radius of the dust particle, ϵ' and ϵ'' are dielectric constants measured from saline dust storms. A detailed discussion on particulate scattering is found in [14] and [13].

2.1.2.5 Refractive Effects and Scintillation

Temperature and pressure variations result in different advective (horizontal) and convective (vertical) velocities of various layers in the atmosphere. This results in inhomegeneity of the atmosphere and thus, different sections of the atmosphere have different refractive indices. Two important phenomena that arise out of refractive effects are multipath fading and error-angle fading.

Multipath fading occurs when the receiver receives multiple copies of the same signal, each delayed by a different amount. This phenomenon is not significant in short path lengths, but should be accounted for when path lengths exceed three km [15]. As the signal travels from one point to another, the spread beam passes through various layers of the atmosphere with different refractive indices. When the distance is greater, the beam-spreading is greater and the number of layers

traversed by the signal components becomes greater. Therefore, multipath effects are greater at longer lengths.

Error-angle fading, or beam-whipping, happens when the displacement of the beam from the center of the receiving antenna becomes so large that the receiver completely misses the signal.

Scintillation is defined as the short-term variations of refractive index associated with air turbulence. A prediction method for calculating statistical properties of signal fluctuations due to scintillation is presented in [16].

2.1.2.6 Rain Attenuation

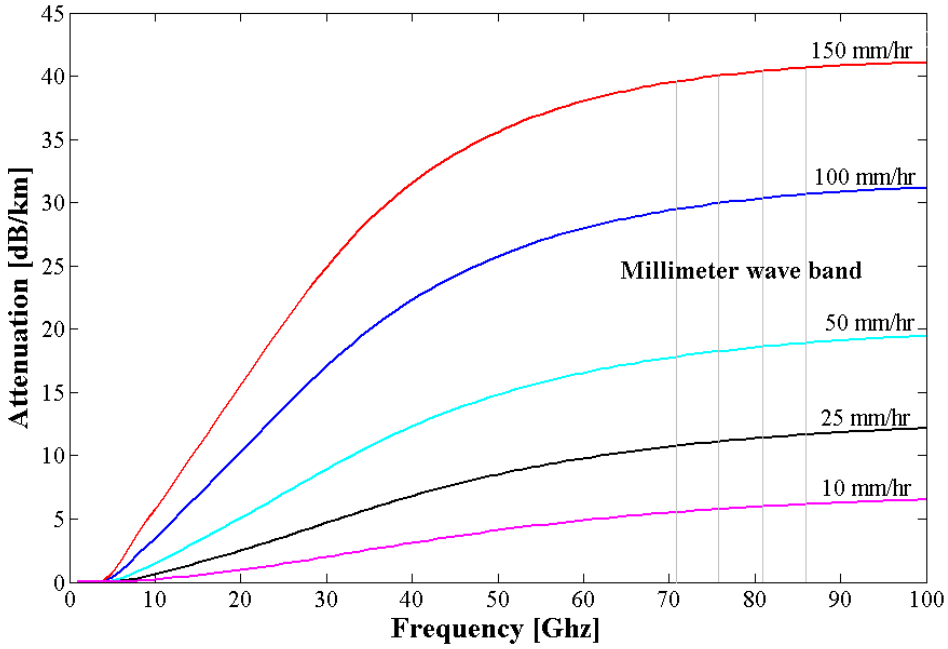

Figure 2.3. Frequency vs. attenuation

Rain fading is the most dominant of all the factors contributing to atmospheric attenuation. This is because the size of rain drops is comparable to the

wavelengths of MWB signals, which causes scattering of the signal. Attenuation due to rain is dependent on the size of rain drops, rain rate, velocity, and polarization of rain drops. Of these, rain rate is the principal factor that decides the extent of attenuation. Very light rain affects link performance marginally, while heavy rains can completely degrade link performance. Figure 2.3 shows the attenuation due to rain at various millimeter wave frequencies, obtained using the ITU-R P.838-3 curves (explained in Section 2.2.1.2). Figure 2.4 shows the attenuation due to rain in MWB. Link planners use measurements of rain rate in a particular region and plots such as the one shown in Figure 2.3 to predict outages due to rain. Attenuation data are not as readily available as rainfall data. So, a relationship like this will be useful for predicting attenuation given the rainfall statistics of a region. Empirical formulae have been developed based on measure-

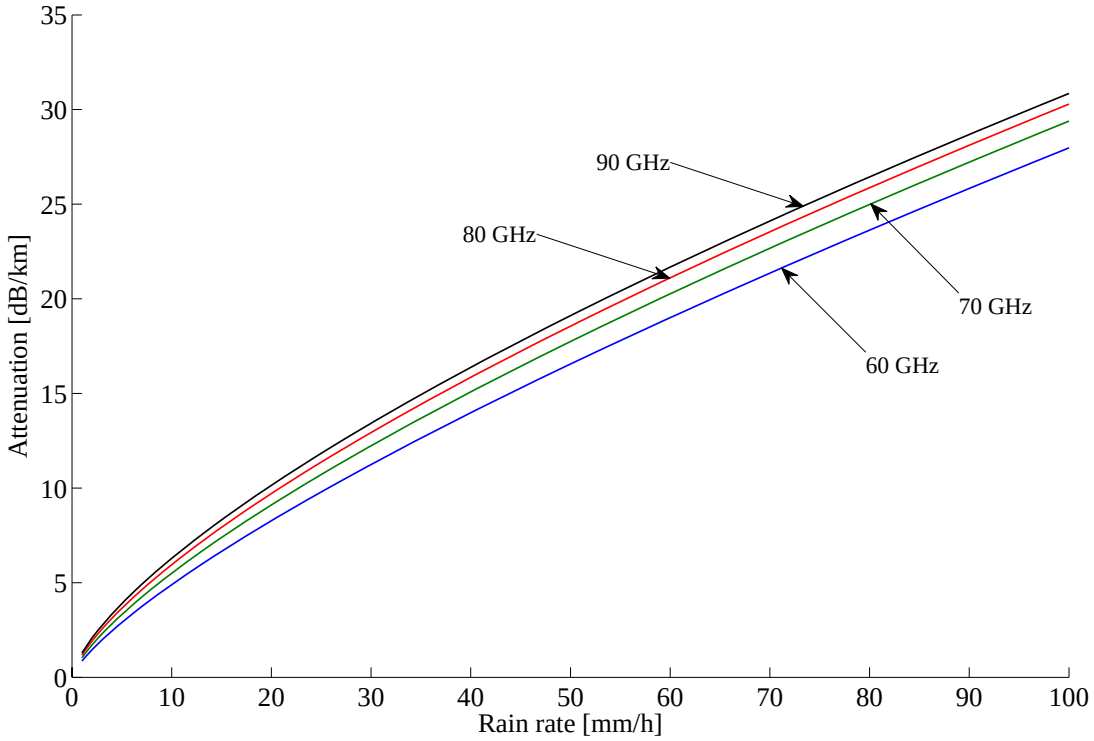

Figure 2.4. Rain rate vs. attenuation

ments of rainfall and attenuation. Two such models are the Crane model and the ITU-R P. 838-3 model. These are explained in detail in the following sections.

2.2 Related Work

This section discusses work done in modeling rain attenuation, storm modeling, and link modeling at millimeter wave frequencies.

2.2.1 Modeling Attenuation due to Rain

This section deals with the measurement of attenuation due to rain, channel modeling in millimeter wave frequencies and network planning considerations in literature.

The effects of rain on MWB transmissions have been studied for decades with results published relating attenuation and rain rate. There are two approaches to modeling attenuation due to rain: developing analytical models based on physical phenomena and building empirical models based on measurements. Due to multiple atmospheric factors contributing to attenuation, it is difficult to develop an analytical model based on the physics of the phenomena. On the other hand, empirical models are more practical to develop and are reasonably accurate in predicting the long-term effects of rain and other atmospheric phenomena on millimeter wave transmissions [17], [18] and [4]. Two models widely used in designing millimeter wave systems are the Crane model and the ITU-R P.838-3 model. Both the models use"rain-zones", or areas in which long term statistics of rain are correlated. Each zone corresponds to a standard set of coefficients that are used in calculating attenuation due to rain. Figure 2.5 shows the Crane zones in the US.

These two methods are next discussed briefly, followed by millimeter wave

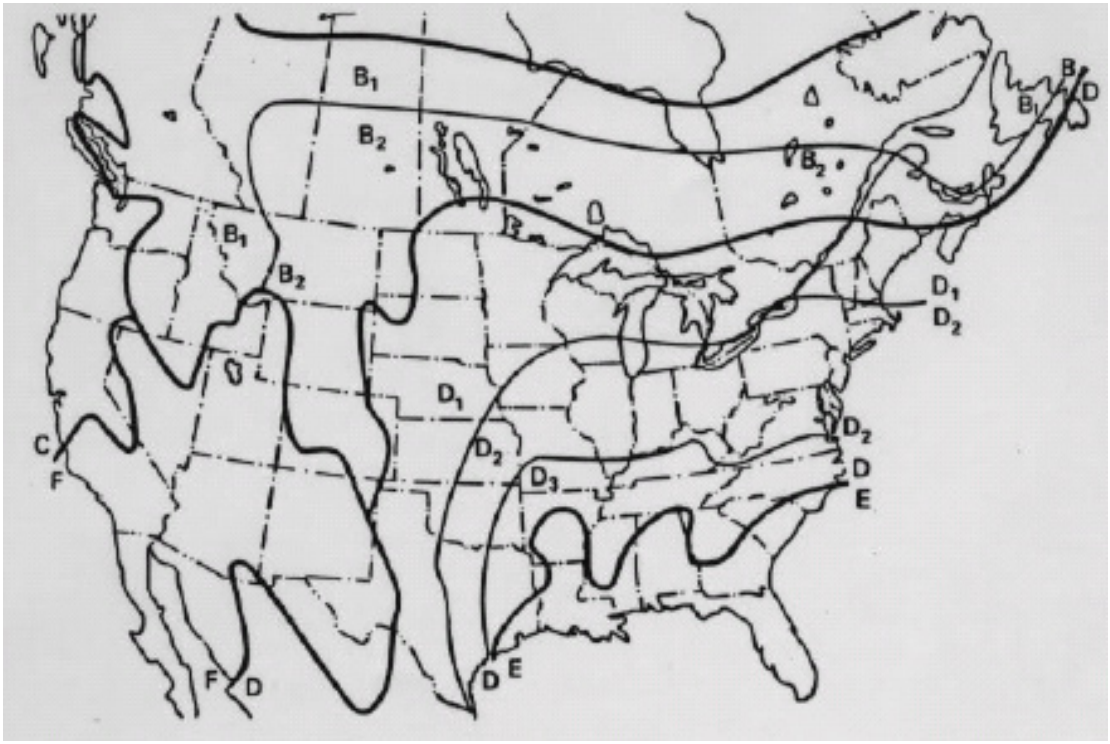

Figure 2.5. Crane rain zones in the US [2]

channel modeling research and storm modeling studies.

2.2.1.1 Crane Model

Robert. K. Crane developed the global (Crane) model for rain attenuation in 1980. It was based "entirely on geophysical observations of rain rate, rain structure, and the vertical variation of atmospheric temperature" [19]. Attenuation is calculated from rain rates using [20]:

$$A(R_p, D) = \alpha R_p^{\beta} \left[\frac{e^{u\beta d} - 1}{u\beta} - \frac{b^{\beta} e^{c\beta d}}{c\beta} + \frac{b^{\beta} e^{c\beta D}}{c\beta} \right], \qquad d \leqslant D \leqslant 22.5 \text{ km} \tag{2.8}$$

$$A(R_p, D) = \alpha R_p^{\beta} \left[\frac{e^{u\beta D} - 1}{u\beta} \right], \; 0 \;\; < \;\; D \;\leqslant\; d \tag{2.9}$$

where A is the signal attenuation in dB, D is the rain affected path length, R_p is the rain rate in mm/h, α, and β are numerical constants, and u, b, c, and d are empirical constants defined as:

$$u = \frac{\ln(be^{cd})}{d}$$
$$b = 2.3R_p^{-0.17}$$
$$c = 0.026 - 0.03 \ln R_p$$
$$d = 3.8 - 0.6 \ln R_p.$$

In 1982, Crane proposed the two-component rain attenuation model based on "the observations of volume cells and debris and an ad hoc procedure to account for the spatial correlations for each component" [19]. It was revised in 1989 and is called the revised Crane two-component model.

2.2.1.2 ITU-R P.838-3

The International Telecommunication Union (ITU) outlines a procedure to calculate attenuation from rain rates in ITU-R P.838-3. According to the recommendation, attenuation is given by [21]:

$$\gamma_R = kR^{\alpha} \tag{2.10}$$

where γ_R is the attenuation in dB/km, R is the rain rate in mm/h, and k and α are obtained from the following equations:

$$\log_{10} k = \sum_{j=1}^{4} a_j \exp\left[-\left(\frac{\log_{10} f - b_j}{c_j}\right)^2\right] + m_k \log_{10} f + c_k \tag{2.11}$$

$$\alpha = \sum_{j=1}^{5} a_j \exp\left[-\left(\frac{\log_{10} f - b_j}{c_j}\right)^2\right] + m_\alpha \log_{10} f + c_\alpha \tag{2.12}$$

where f is the frequency in GHz, k is either k_H or k_V, α is either α_H or α_V. k_H and α_H are constants for horizontal polarization and k_V and α_V are constants for vertical polarization. For linear and circular polariation, k and α are obtained from the following equations:

$$k = [k_H + k_V + (k_H - k_V)\cos^2\theta\cos 2\tau]/2 \tag{2.13}$$

and

$$\alpha = [k_H\alpha_H + k_V\alpha_V + (k_H\alpha_H - k_V\alpha_V)\cos^2\theta\cos 2\tau]/2\text{k} \tag{2.14}$$

where θ is the path elevation angle ($\theta = 0$ for terrestrial paths) and τ is the polarization tilt angle relative to the horizontal. Equations 2.11 and 2.12 were developed from "curve-fitting to power-law coefficients derived from scattering calculations" [21]. Table 2.3 compares the ITU and Crane models [4].

Table 2.3. Attenuation at 99.99% availability for a 3 km link [4]

ITU Zone/Crane Zone	**Units**	**E/F**	**D/C**	**K/D2**	**N/E**
Rain rate ITU/Crane	mm/hr	22/22	19/29	42/47	95/91
ITU-R 530	dB	10.8	14.3	22.3	39.2
Crane global	dB	13.2	17.2	25.7	45.9
Crane 2-component(TC)	dB	13.6	18.4	28.8	52.0
Crane revised TC	dB	12.4	20.0	26.9	51.3

It is seen from Table 2.3 that the Crane models are a little pessimistic relative to the ITU model in that they suggest higher attenuation for the same value of rain rate. The ITU model is used in this work for calculating attenuation due to rain, since it is an international standard. Furthermore, manufacturers of MWB equipment use the ITU model to design their links [22] .

2.2.2 Link Modeling

In this section, background that deals with link modeling in the millimeter wave range and modeling of storm structures is presented.

A number of models have been described in literature about modeling links affected by rain. These are either variants of the Crane/ITU model, or Markov models built from measurement of rain and attenuation over time, or a combination of both.

Hendrantoro et al. [23] propose a multivariate autoregressive model for rain attenuation and simulate it on two short links operating at 30 GHz. An autoregressive model of rain attenuation is built using spatial and temporal measurements of rainfall and attenuation. This model can be used to simulate rain events on a network with short links that show significant correlation in the rain rates they see. The spatio-temporal characteristics of rainfall must be known at both sites. This model is highly location specific like most others.

Dissanayake et al. [24] discuss a method to quantify the combined effect of various atmospheric phenomena on Ka-band links. Rain attenuation, cloud attenuation, gaseous absorption, melting layer attenuation, and refractive effects are combined to give a single value of attenuation.

Utsunomiya and Sekine [25] discuss attenuation at millimeter and sub millime-

ter wavelengths. They compare attenuation due to rain using several drop size distributions and declare that a Weibull distribution yields best results.

Alasseur et al. [26] discuss a couple of methods to model rain-rate time-series for attenuation calculations. Both methods employ heirarchical Markov chains: the outer chain deciding if there is rain or not (duration of rain events) and the inner chain deciding the intensity of the rain if present.

2.2.3 Storm Modeling

Montopoli et al. [27] characterize the shape of rain storms using C-band radar data. They model horizontal profiles of rain cells using three analytical models and measurements from radar.

Fontan et. al. [28] propose a technique to convert rain-rate series to attenuation series using a synthetic storm technique. They evaluate their technique on an event-by-event basis using a 40 GHz satellite link. Their model involves simulating rain events of two types: quasi-flat and spiky. The former is a longer event and has moderate rainfall associated with it. The latter is short but is associated with heavy rainfall.

Daru et al. [29] investigate the space and time correlation of rain attenuation based on measurements made using a network that has star topology. They present measurements taken from links in Hungary and a correlation analysis of rain attenuation across multiple links within a geographical area. Spatial correlation as a function of angular seperation between the links is plotted. This work quantifies the space and time correlation of rain attenuation based on measurements, but does not propose techniques to simulate the effects of rain.

Riva [30] reviews state-of-the-art research in the field of spatial distribution of

propagation parameters affecting millimeter wave band frequencies. He characterizes properties of rain cells like shape, peak intensity, dimension, and movement direction and speed. Rain cells are elliptically modeled and cell diameter distribution of oceanic and land rain cells is presented.

Most of these papers discuss means to obtain time-series values of attenuation given the rain-rate statistics of a region using a reference model such as the Crane model or the ITU-R model. Very few discuss the spatial characterization of storms and how to extract spatial correlation of rain attenuation given the geometry of the storm. This thesis proposes a method to calculate attenuation due to rain on links given the structures and positions of storm cells. Though it does not provide a closed form expression for spatial correlation, the results can be used to simulate the effects of rain on a mesh network or in dynamic routing schemes where knowledge of attenuation is required in real time.

Chapter 3

Synthetic Storm Modeling

This chapter deals with synthetic storm modeling, which involves characterizing the properties of a real-world storm to make it suitable for use in network simulations. This involves defining the structure of the storm including the cells within the storm, as well as modeling the movement of the storm system. It also involves quantifying the effects of the storm system in terms of FER (frame error rate).

This chapter is organized as follows: A geometric model of the storm system is built (Section 3.1.1), its movement through the fixed wireless network is simulated (Section 3.1.2), length (l) in km of the affected links is computed (Section 3.2.1), and attenuation (γ) in dB/km is calculated by using the equations outlined in Section 2.2.1.2 (Section 3.2.2). The product of γ and l gives the attenuation across any link at any time t.

The chief assumption in calculating attenuation along a link is that the LOS component of the beam is a straight line. This is a valid assumption given the fact that the center of the beam has the strongest signal component and with a beamwidth of 1.2°, the signal components farthest away from the center are

the weakest. So, for the purpose of attenuation calculations, the beam can be assumed to be a straight line. In other words, only the LOS component is taken into consideration, neglecting the effect of secondary waves.

3.1 Geometric Modeling

This section characterizes storm properties such as shape and trajectory. Section 3.1.1 describes the structure and composition of the storm. Section 3.1.2 discusses the trajectory of the storm system.

3.1.1 Storm Geometry

The structure of a storm cell can be best approximated by an ellipsoid [27, 31, 32] whose two-dimensional footprint is an ellipse. Figure 3.1 shows an ellipse labelled with the model parameters. A two-level heirarchical model is used in which the cells are inner ellipses of greater rain intensity and the system is the outer ellipse of lesser intensity. The cells are non overlapping and completely contained within the system. The storm with n ellipses is defined as:

$$C = \{(a_i, b_i, \theta_i), h_{i,t}, k_{i,t}, R_i, \mathbf{v}\} \tag{3.1}$$

where a_i is the semimajor axis of ellipse i, b_i is the semiminor axis of ellipse i, $h_{i,t}$ is the x coordinate of the center of ellipse i at time t, $k_{i,t}$ is the y coordinate of the center of ellipse i at time t, θ_i is the angle in radians the major axis of ellipse i makes with the positive x-axis, R_i is the rain rate associated with ellipse i in mm/h, and $\mathbf{v}$ is the velocity of the storm system in km/h.

Using the standard equation for an ellipse, each ellipse in the storm system is

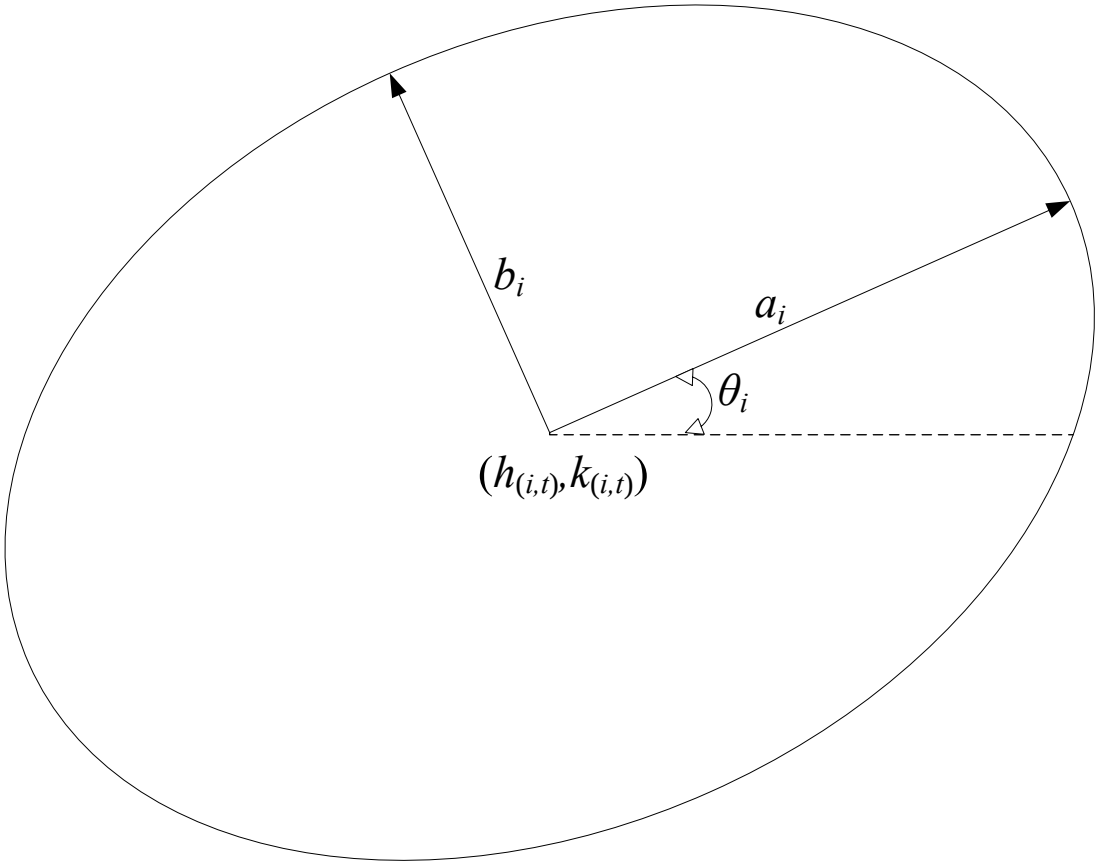

Figure 3.1. Elliptical modeling of storm

represented by:

$$\frac{((x-h_{i,t})\cos\theta_i + (y-k_{i,t})\sin\theta_i)^2}{a_i^2} + \frac{((y-k_{i,t})\cos\theta_i - (x-h_{i,t})\sin\theta_i)^2}{b_i^2} = 1 \tag{3.2}$$

Equation 3.2 is obtained by making the following transformations:

$$x' = x - h_{i,t}; \quad y' = y - k_{i,t}$$

$$x'' = x'\cos\theta_i + y'\sin\theta_i; \quad y'' = y'\cos\theta_i - x'\sin\theta_i$$

to the equation of an ellipse centered at (0,0):

$$\frac{x^2}{a^2} + \frac{y^2}{b^2} = 1$$

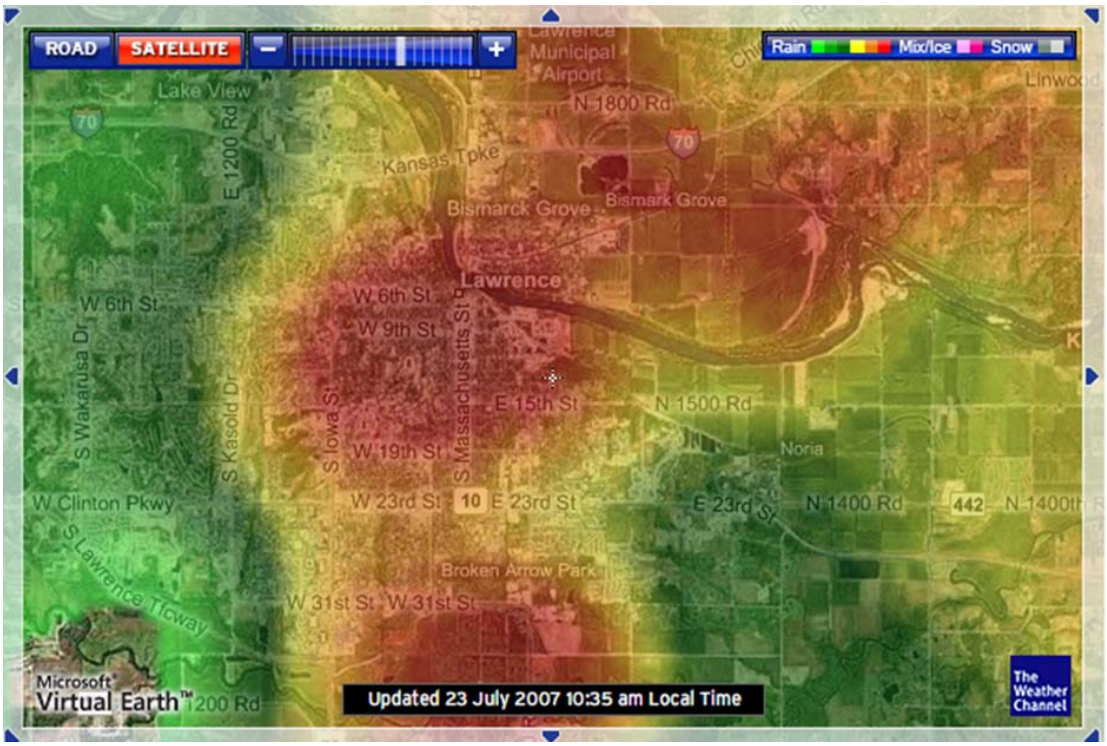

Figure 3.2. Radar image with light and heavy rain zones

Figure 3.2 shows an image of a storm system that shows cells with varying rain intensities. The red portions (dark in the center of the figure) indicate presence of heavy rain and the yellow (light) portions have lighter rain. Figure 3.3 is a very rough approximation of the radar image with ellipses replacing the red and yellow zones. R_i is the rain rate associated with the inner ellipses and R_S is the rain rate associated with the larger outer ellipse. $R_S < R_i \ \forall \ i$.

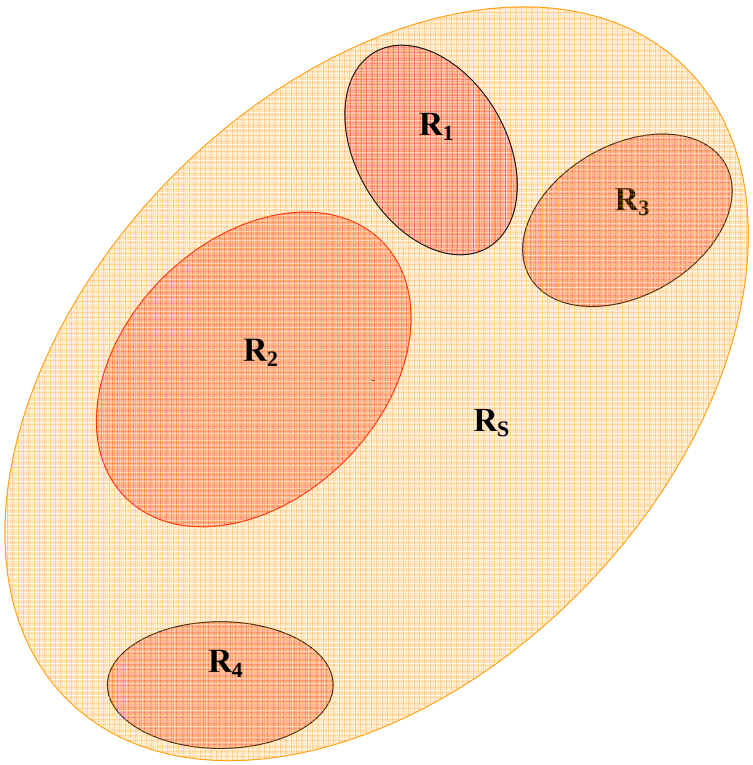

Figure 3.3. Elliptical modeling of radar images

3.1.2 Storm Movement

The system of ellipses is assumed to move together, in particular, the x and y coordinate offsets of the centers of the cells within the system remain the same over time. Hence, the trajectory of the system is the trajectory of the collection of ellipses. The trajectory of the system is defined by a quadratic equation of the form:

$$Ax^2 + By^2 + Cx + Dk + E = 0 \tag{3.3}$$

A quadratic equation in x and y can be used to represent a conic-section curve or a straight line, depending on the values of the coefficients of x and y. The center

of the system (h_t,k_t) at any instant t is obtained from the solutions to Equation 3.3. ($h_t \pm \Delta x_i$,$k_t \pm \Delta y_i$) gives the center of cell i where Δx_i is the x coordinate offset from h_t and Δy_i is the y coordinate offset from k_t.

Figure 3.4 shows the movement of a storm across an 8×8 square mesh network and Figure 3.5 shows the movement of a storm across an arbitrary mesh network with 6 nodes.

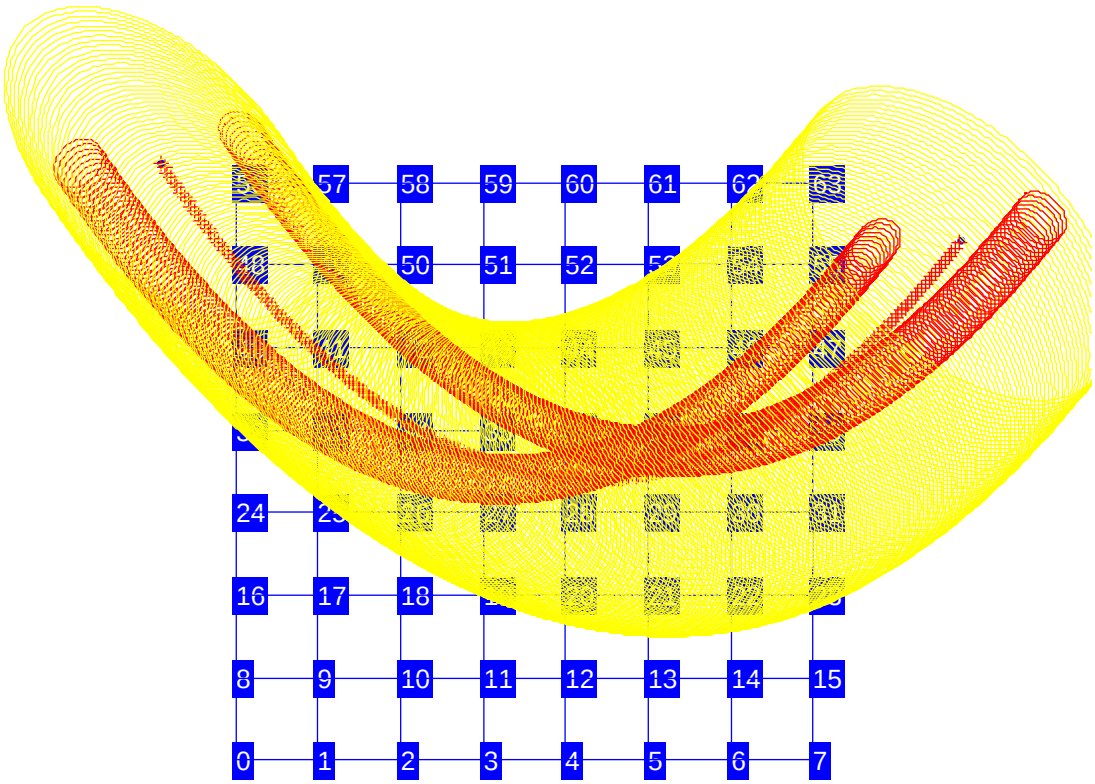

Figure 3.4. Storm movement generated in an 8×8 mesh

3.2 Link Attenuation

From the storm structure and trajectory, the position of the storm ellipses at every instant t is known. The coordinates of the nodes are specified and the lines

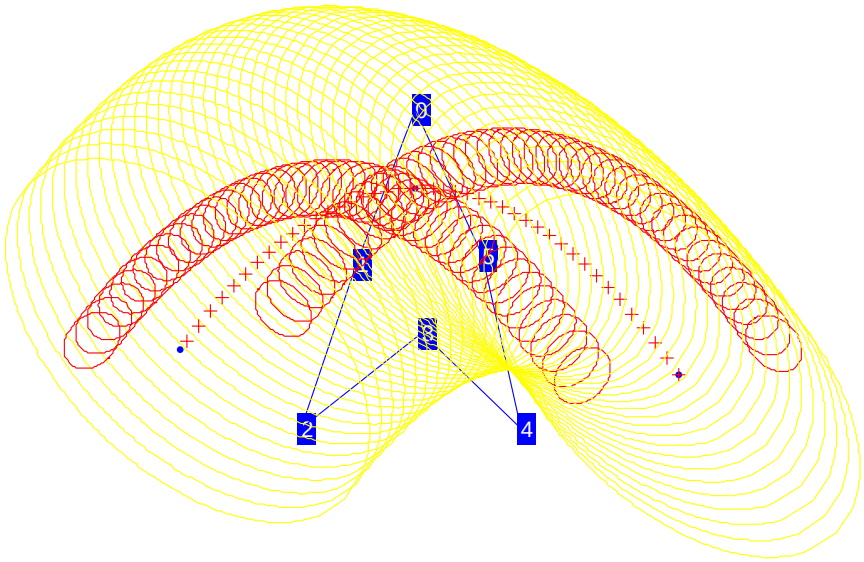

Figure 3.5. Storm movement in an arbitrary mesh with 6 nodes

between them represent the links. The question of what is the attenuation due to rain on the link is reduced to the problem of finding the points of intersection of the link on the ellipse and calculating how much attenuation is suffered by that section of the link intersecting a cell. This section explains the calculation of portions of the links affected, followed by attenuation calculations.

3.2.1 Calculation of Fraction of Links Affected

Due to the "pencil beam" characteristics of millimeter waves, it is assumed that the beam is a straight line for the purpose of computation of portions of

links affected by rain. The next step is to determine whether each link is under a storm cell and to compute the intersecting portion. For this, the equation of the link is determined from the end points of the link:

$$\frac{y - y_1}{y_2 - y_1} = \frac{x - x_1}{y_2 - y_1} \tag{3.4}$$

where the tuples (x_1, y_1) and (x_2, y_2) are the coordinates of the end points of the link.

Each storm cell has its own equation presented already in 3.1,

$$\frac{((x - h_{i,t})\cos\theta_i + (y - k_{i,t})\sin\theta_i)^2}{a_i^2} + \frac{((y - k_{i,t})\cos\theta_i - (x - h_{i,t})\sin\theta_i)^2}{b_i^2} = 1 \tag{3.5}$$

Equations 3.4 and 3.5 are solved and solutions are obtained for either x or y which could be one of the following three cases:

1. imaginary roots – no intersection
2. real and equal roots – link tangential to cell
3. real and unequal roots – link and cell intersect

It should be noted that a line segment itself is not defined by an equation, but it is the line containing the segment that is. Hence, having affirmed that there is an intersection between the ellipse and the link if it were infinitely long, the next step is to see if it actually affects the link of finite length. If the line is tangential, the length of the link affected by the storm, and hence the attenuation is zero. For the case where the roots are real, the following three cases are possible depending on the dimensions of the ellipse and the length of the link:

1. the link is completely encompassed by the cell (Figure 3.6)

2. the cell covers a portion of the link on either side (Figure 3.7)

3. the cell is across the link (Figure 3.8)

If the end points of the link are **A** and **B** and the end points of the chord along the link on the ellipse are **C** and **D**, by comparing the distances between these points, the position of the cell footprint with respect to the link can be found. For example, if the link were to be completely encompassed by the cell as shown in Figure 3.6, then $\overline{\mathbf{CA}} + \overline{\mathbf{AD}} = \overline{\mathbf{CD}}$ and $\overline{\mathbf{CB}} + \overline{\mathbf{BD}} = \overline{\mathbf{CD}}$. The dashed line represents the link and the dotted line is the line containing the link. These

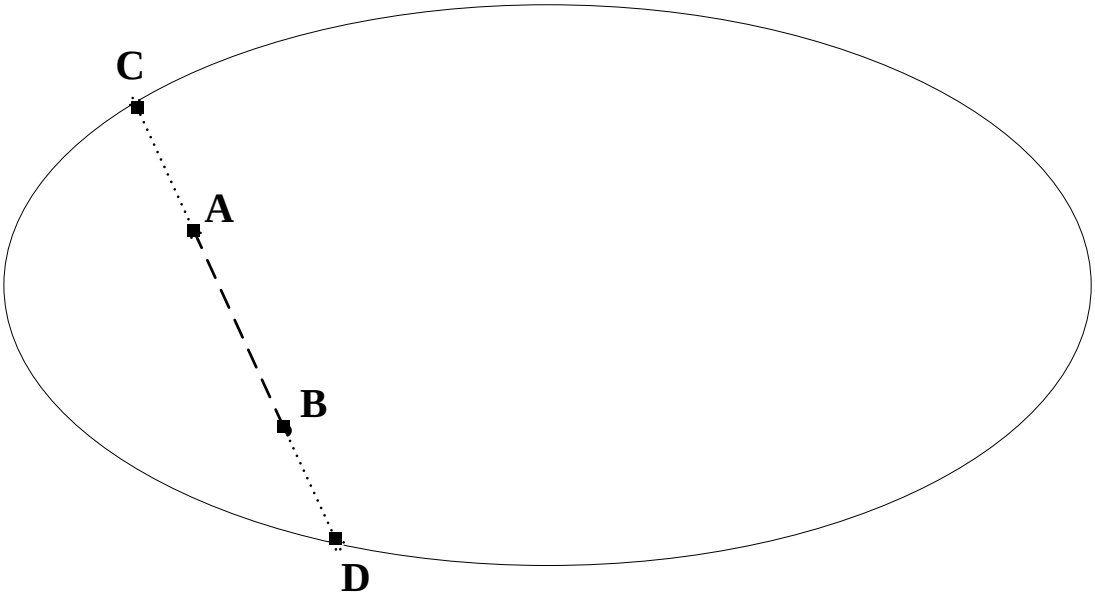

Figure 3.6. Link entirely encompassed by the cell

conditions do not hold for any other positions of **A**,**B**,**C**, and **D** except in the case that **C** and **D** are the same point, in which case, the cell is tangential to the link. Figures 3.7 and 3.8 show the other two cases.

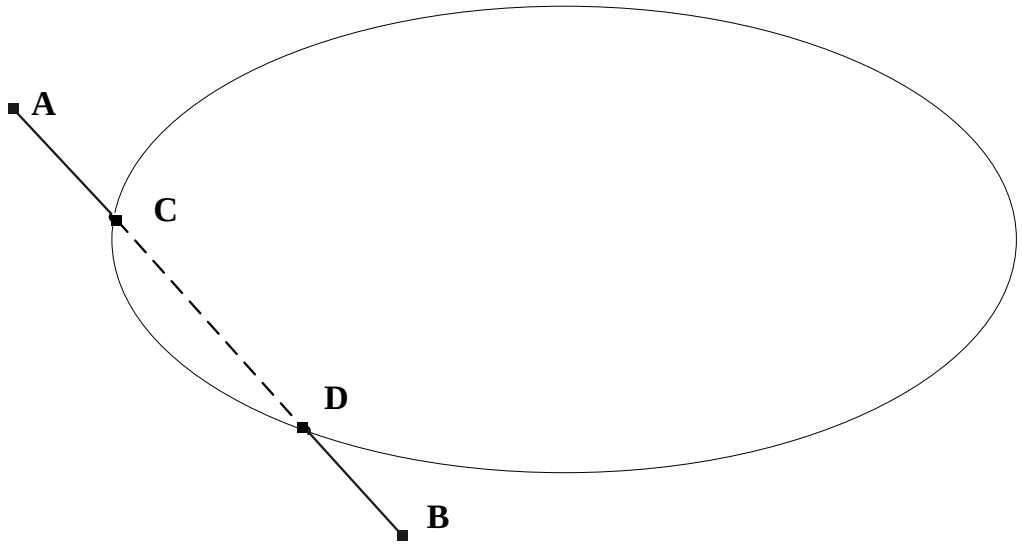

Figure 3.7. Fraction of the link affected by the cell

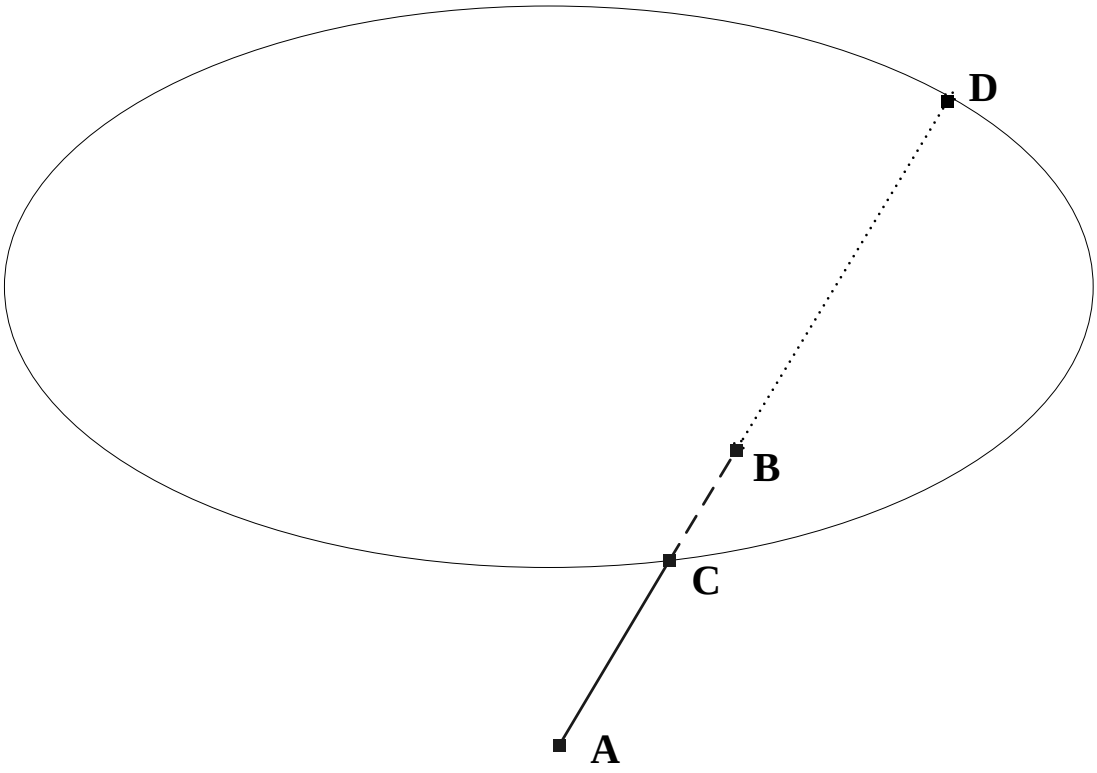

Figure 3.8. Link covered at one end by the cell

By looking at all intersection possibilities for each link and each storm cell, we can determine which links are affected at a particular position of the storm and how much those links are affected. From this, the cumulative attenuation on each link is calculated. This translates into a bit error rate value that is then input into ns-2 network simulations, as described in Chapter 4.

3.2.2 Attenuation on Affected Links

A key problem consists of calculating the attenuation of a link given that it is intersected by a storm cell. Given the rain rate associated with a cell and the frequency of operation of the transceivers, attenuation in dB/km can be calculated as outlined in 2.2.1.2. If there are m links, the effective attenuation along link i at any time t is given by

$$\Gamma_i(t) = \gamma_{S,i} d_{S,i} + \sum_{j=1}^{n} \gamma_{j,i} d_{j,i} - \sum_{j=1}^{n} \gamma_{S,i} d_{j,i} \tag{3.6}$$

where, $\Gamma_i(t)$ [dB] is the effective attenuation due to rain along link i at time t, $\gamma_{S,i}$ [dB] is the attenuation due to the bigger ellipse on link i at time t, $d_{S,i}$ [km] is the length of link i affected by the big ellipse at time t, $\gamma_{j,i}$ [dB] is the attenuation due to cell j on link i at time t, $d_{j,i}$ [km] is the length of link i affected by cell j at time t, n is the number of cells in the storm system, and $i = \{1 \ \ to \ \ m\}$.

From the attenuation values, received energy (per bit) to noise ratio is calculated using:

$$\left(\frac{E_b}{N_0}\right)_{i,\text{rain}-\text{event}} = \left(\frac{E_b}{N_0}\right)_{i,\text{blue}-\text{sky}} - \Gamma_i \tag{3.7}$$

where $\left(\frac{E_b}{N_0}\right)_{i,\text{rain}-\text{event}}$ is the energy (per bit) to noise ratio on link i during a

rain event and $\left(\frac{E_b}{N_0}\right)_{i,\text{blue}-\text{sky}}$ is the energy (per bit) to noise ratio on link i during clear sky conditions.

Then, bit error rate (BER) is calculated from E_b/N_0 using:

$$\text{BER} = q\left(\sqrt{\left(\frac{E_b}{N_0}\right)_{i,\text{rain}-\text{event}}}\right) \tag{3.8}$$

The FER (frame error rate) is obtained from the BER using the approximation [33]:

$$\text{FER} = (1 - (1 - \text{BER})^n) \tag{3.9}$$

where n is the number of bits per frame transmitted. Equation 3.9 assumes that the errors are independent and identically distributed. Typically, BER or FER requirements for the normal operation of a link are specified for link budgeting purposes. BER for the on-off keying (OOK) modulation scheme used commonly in MWB radios is defined as:

$$\text{BER} = q\left(\sqrt{\left(\frac{E_b}{N_0}\right)_{\text{blue}-\text{sky}}}\right) \tag{3.10}$$

Rearranging the terms in Equation 3.10, received E_b/N_0 in dB given BER for normal operation in blue sky conditions is obtained:

$$\left(\frac{E_b}{N_0}\right)_{\text{blue}-\text{sky}} = 20 \times \log q^{-1}(\text{BER}) \tag{3.11}$$

If the specified BER requirement is 10^{-10}, the corresponding blue sky E_b/N_0 is 36 dB.

Figure 3.9 shows the relationship between FER and rain rate for a one mile (1.6 km) long link. The relationship is based on the received E_b/N_0, length of the link,

and the number of bits per frame transmitted. Figure 3.10 depicts FER vs. rain rate for a five mile (eight km) long link that is used to formulate the Markov model explained in Chapter 5. It is seen that the longer the link, the more severe the attenuation.

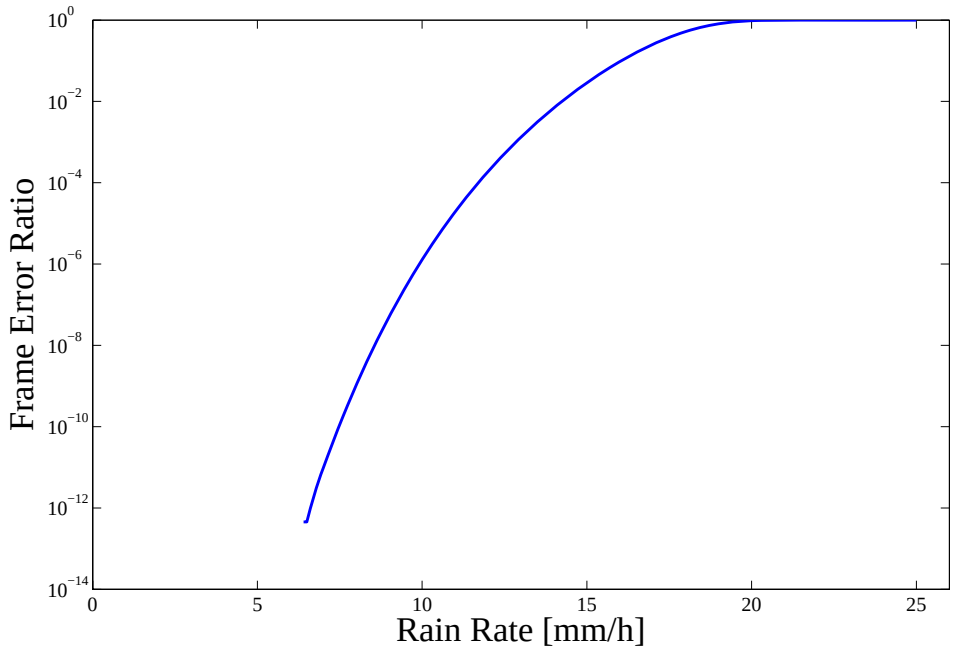

Figure 3.9. FER vs. rain rate for a 1 mile link at 73.5 GHz

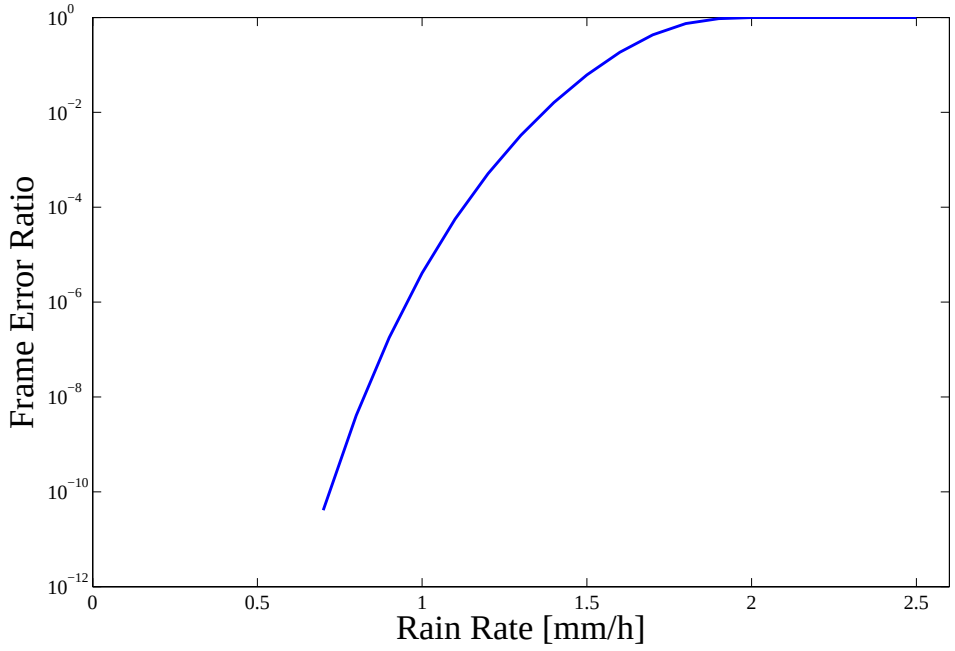

Figure 3.10. FER vs. rain rate for a 5 mile link at 73.5 GHz

Chapter 4

Mesh Network Simulation

Chapter 3 explains a method to quantify the spatio-temporal effects of rain on MWB links. To be practically applicable, it must work in tandem with a simulation to obtain the consequences of a weather event on network performance. This is done using the ns-2 simulation package [7]. The results of the loss calculations detailed in Section 3.1 are input into a mesh-network simulation to obtain results of the interaction of the weather event with the network.

This chapter is organized as follows: the storm model is described in Section 4.1. Section 4.2 describes the network model and simulation parameters. Finally, Section 4.3 presents and analyzes the results of the simulations.

4.1 Simulation Model

Synthetic storms are generated using the methodology explained in Section 3.1 and trace files are produced which are then input into ns-2. The two-level heirarchical storm model is used. The parameters of the storm are chosen such that the smaller ellipses are completely contained within the bigger ellipse and

the rain rates associated with the smaller ellipses are greater than the rain rate of the bigger ellipse. Three different cases with varying ellipse geometries and trajectories are simulated from which throughput and carried load are obtained.

4.1.1 Storm Structure

For the first two simulation cases, the outer ellipse has a major-axis diameter of 30 km and minor-axis diameter of 10 km, the inner ellipses have major-axis diameters of seven km, minor-axis diameters of three km and have centers that are slightly offset from the center of the outer ellipse so that they do not intersect one another or the bigger ellipse. For the third case, the outer ellipse has a major-axis diameter of 30 km and minor-axis diameter of 20 km, inner ellipses have major-axis diameters of nine km and minor-axis diameters of five km. In all the cases, the rain rate of the bigger ellipse is a light two mm/h and the rain rate of the smaller ellipse is a heavy 10 mm/h.

4.1.2 Storm Patterns

Two different storm patterns are generated and their effects are simulated. The first one passes through an edge of the square mesh while the second passes along the principal diagonal of the mesh. Figures 4.2 and 4.6 show the patterns used in the simulation.

4.2 Network Simulation and Parameters

This section discusses the simulation setup in ns-2: topology, node properties, link properties, and traffic.

4.2.1 Network Topology and Characteristics

A 4×4 mesh network is used for the simulation. The network is shown in Figure 4.1. Each link in the network is modeled as a wired link since this best represents fixed point-to-point wireless links in ns-2. Each link has a bandwidth of 10 Mb/s and has a delay of 30 μs based on the speed-of-light delay at a distance of 10 km. Each node also has a droptail queue.

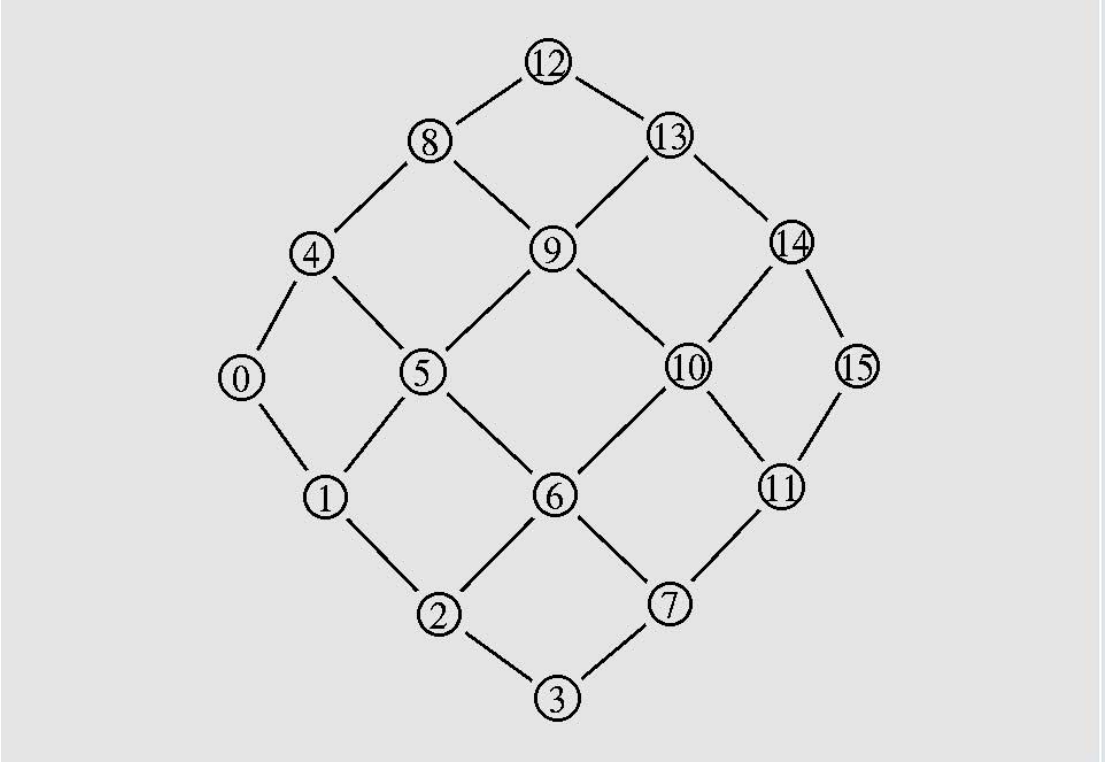

Figure 4.1. Case 1: Topology of the mesh used in simulations

4.2.2 Traffic

The nodes are set up in such a way that every node sends and receives data. This makes the traffic across the network reasonably uniform. Each source sends constant bit rate (CBR) traffic over UDP (user datagram protocol [34]) at 0.8

Mb/s. Source destination pairs are randomly chosen. Therefore, the total traffic on the network is $16 \times 0.8 = 12.8$ Mb/s. Though the capacity of an MWB link is close to one Gb/s, the traffic and the bandwidth are scaled down to permit faster running simulations. This is justified, as we are computing a ratio of recieved packets to sent packets and the relationship is maintained even when the traffic and link rates are scaled down.

4.2.3 Performance Evaluation

To evaluate the performance of the links and network as a whole, the nam visualization and tracegraph tools are used. These are support tools for ns-2 that can graphically illustrate the workings of the network. The loss of affected links is plotted using nam. This shows instantaneous loss across links affected by rain over time.

Throughputs of received and lost bits are plotted using tracegraph. These give an overall picture of how the network as a whole responds to the weather event.

4.3 Results and Analysis

In this section, results of the simulations run with three cases of storm patterns are discussed. The loss-graph of individual links and the throughput plots are analyzed.

4.3.1 Case 1: Vertical Storm Pattern

In this case, the storm moves along the edge defined by nodes 0, 4, 8, and 12. The center of the storm at the beginning of the simulation is at node 12 and it moves towards node 0 in a straight line. Figure 4.2 shows the mesh network and

the structure and trajectory of the storm for Case 1. Each position of the storm is one second apart and the duration of the simulation is approximately 60 seconds.

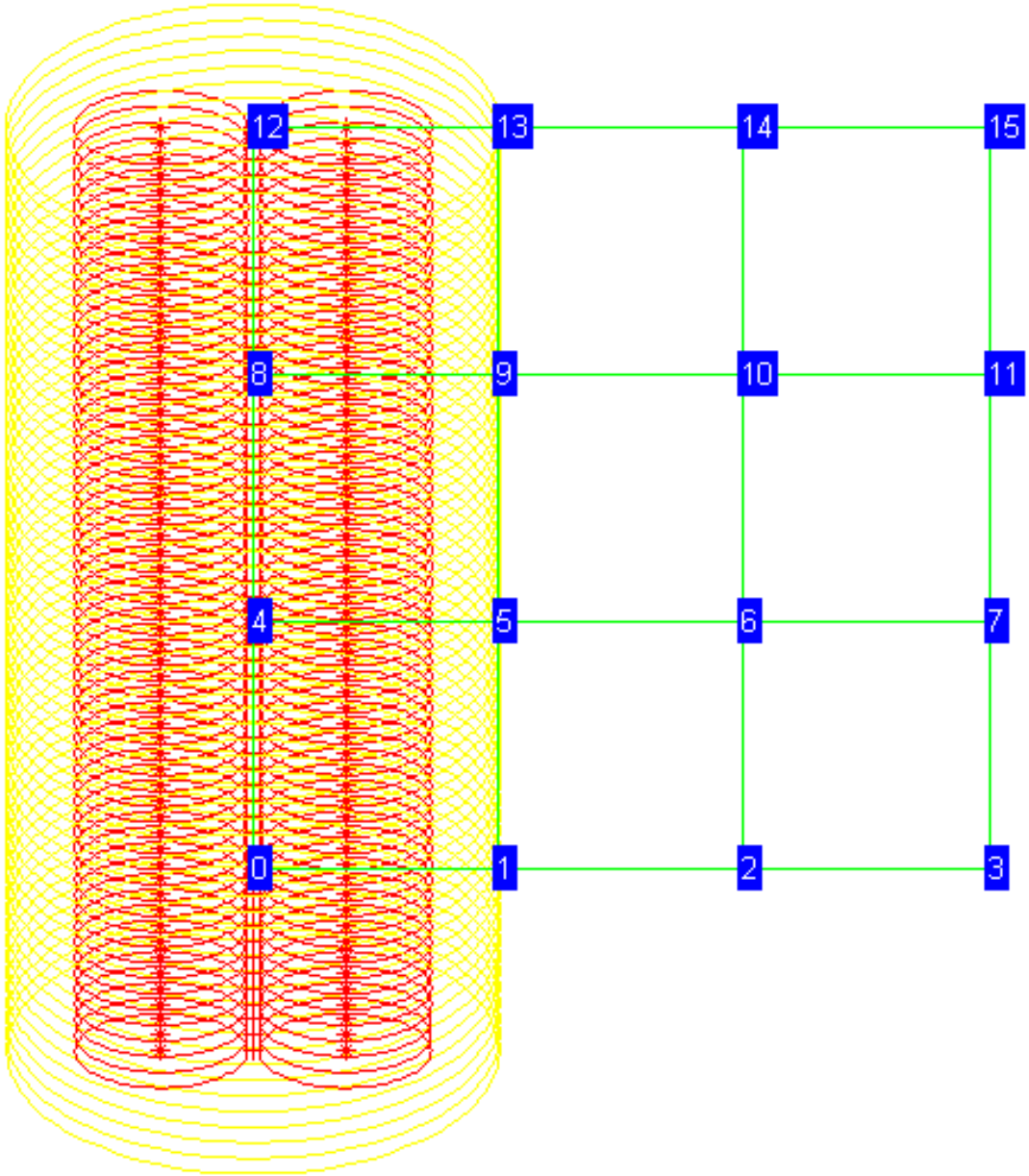

Figure 4.2. Case 1: Storm moves along the edge of a network

Figure 4.3 shows the loss on the affected links, in particular between nodes 12 and 13, 8 and 12, 9 and 8, 8 and 4, 4 and 5, 0 and 4, and 0 and 1.

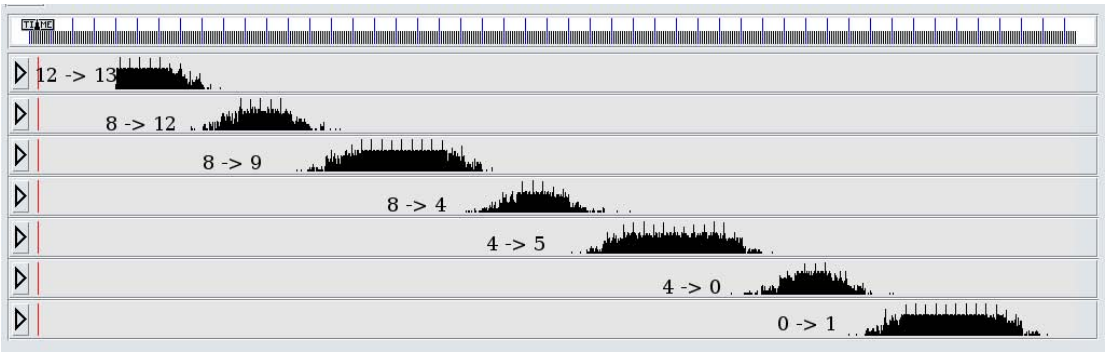

Figure 4.3. Case 1: Packets lost across affected links

The storm enters at node 12 and gradually moves to node 0. The orientation of the inner ellipse is such that it cuts the horizontal links at regular intervals. The vertical edge-links are not affected by the inner ellipses and therefore are under the influence of only the bigger ellipse. As the storm moves in a straight line perpendicular to the x-axis, there is a pattern of losses across links which is clearly seen in Figure 4.3. The link composed of node pair (12,13) gets affected at the beginning of the simulation as the inner ellipse is centered in the middle of the link. The loss on it gradually decreases and finally becomes zero when the storm system has completely passed. The horizontal links (12,13), (8,9), (4,5), and (0,1) show an identical pattern while the vertical links (12,8) (8,4) (12,8) show another pattern albeit identical.

As the storm pattern is regular and most parts of the network are not affected by the storm, the degradation in throughput is of the order of five per cent. From the tracegraph utility, we obtain the number of packets sent (N_s) and the number of packets dropped (N_d). Using this, the carried load of the network (η) can be calculated as:

$$\eta = \frac{N_s - N_d}{N_d} \times 100\% \tag{4.1}$$

For this case, N_s = 171,288 and N_d = 7,728 resulting in a carried load value of η = 95.488%. The average throughput is 11.8 Mb/s compared to 12.8 Mb/s for the ideal case.

Table 4.1. Case 1: Simulation information

Simulation length in seconds:	55.19715
Number of nodes:	16
Number of sending nodes:	16
Number of receiving nodes:	16
Number of generated packets:	176640
Number of sent packets:	171288
Number of forwarded packets:	301392
Number of dropped packets:	7728
Number of lost packets:	2376
Minimal packet size:	500
Maximal packet size:	500
Average packet size:	500
Number of sent bytes:	85644000
Number of forwarded bytes:	150696000
Number of dropped bytes:	3864000
Packets dropping nodes:	0 4 6 12

Table 4.1 shows the details of the simulation for Case 1. Figure 4.4 shows the throughput of all the bits received by all the nodes in the network. It is seen that there is a pattern in the total traffic through the network. Figure 4.5 shows the throughput of all the dropped bits in the network.

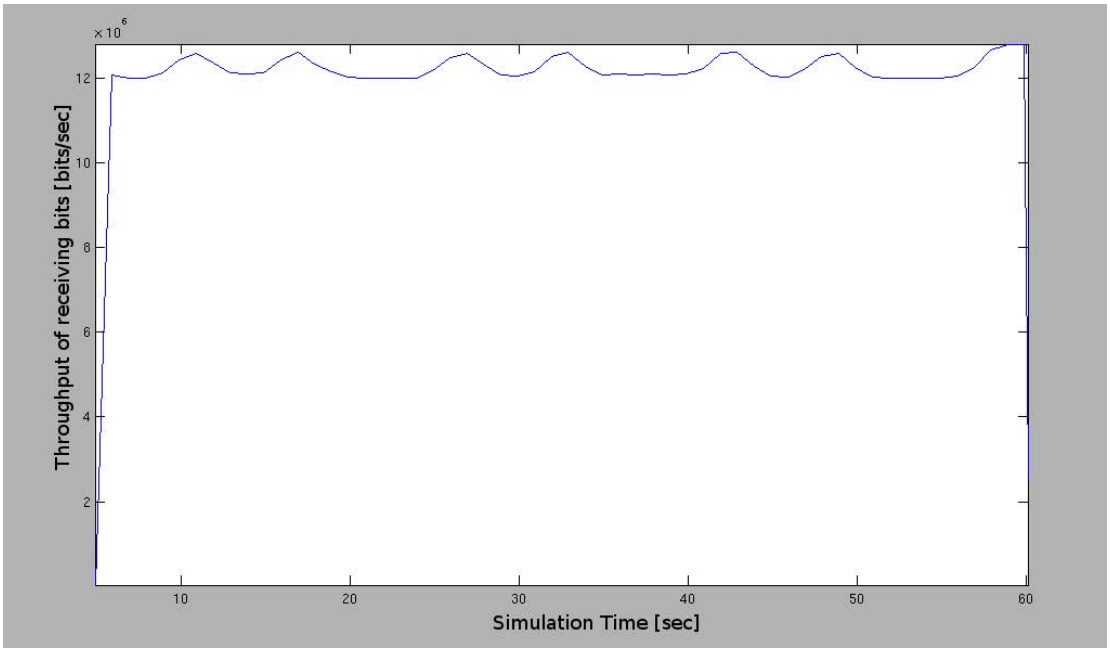

Figure 4.4. Case 1: Throughput of all received bits

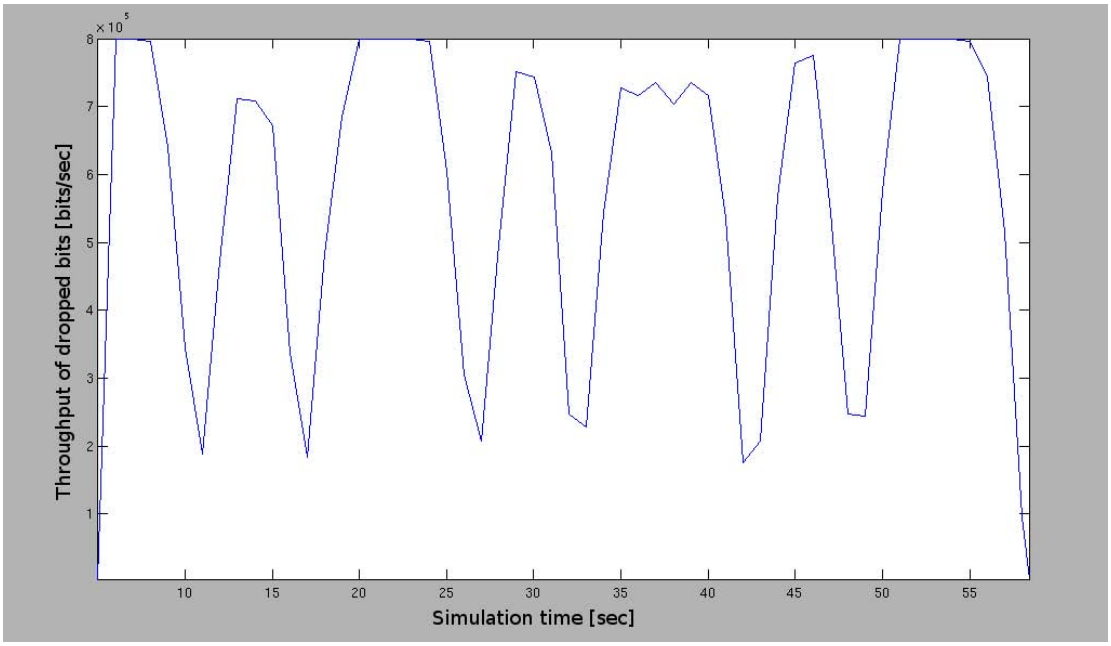

Figure 4.5. Case 1: Throughput of all dropped bits

4.3.2 Case 2: Diagonal Storm Pattern

In this case, the storm starts at node 12 and moves along the principal diagonal to reach node 3 at the end of the simulation. The orientation of the storm cells is

45° with respect to the positive x-axis.

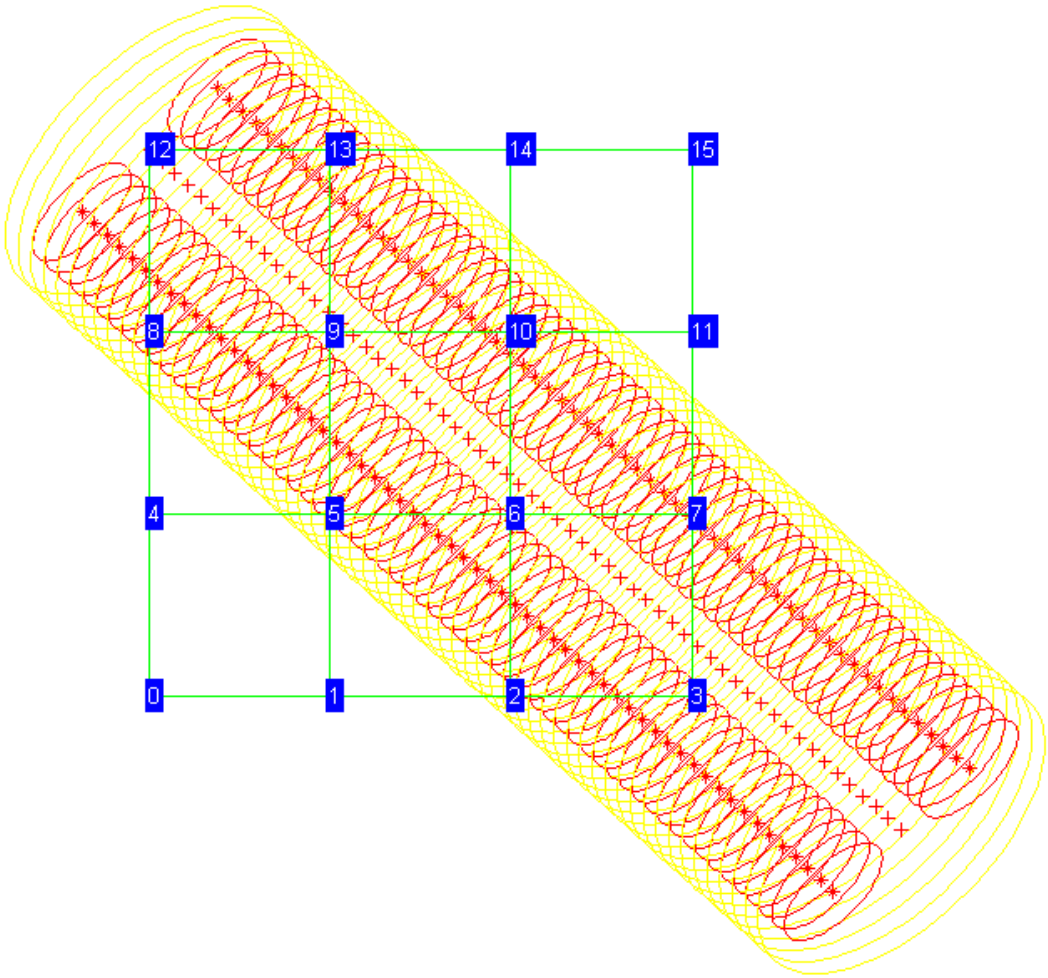

Figure 4.6. Case 2: Storm moves diagonally across the network

Table 4.2 shows the simulation information for Case 2. In this case, N_s = 145,413 and N_d = 15,946, resulting in a carried load value of $\eta = 89.903\%$ which is worse than the first case. This is intuitive because the second storm simultaneously affects more links than the first storm. The average throughput is 10.97 Mbps compared to 12.8 Mbps for the ideal network.

Figure 4.7 shows the throughput of all the received bits and Figure 4.8 shows

Table 4.2. Case 2: Simulation information

Simulation length in seconds:	47.19715
Number of nodes:	16
Number of sending nodes:	16
Number of receiving nodes:	16
Number of generated packets:	151040
Number of sent packets:	145413
Number of forwarded packets:	248374
Number of dropped packets:	15946
Number of lost packets:	10319
Minimal packet size:	500
Maximal packet size:	500
Average packet size:	500
Number of sent bytes:	72706500
Number of forwarded bytes:	124187000
Number of dropped bytes:	7973000
Packets dropping nodes:	2 5 6 8 9 10 12 13

all the dropped bits. These plots are not as intuitive as the ones for the first case because the storm is moving diagonally and the individual cells are aligned at 45° from the positive x-axis.

4.3.3 Case 3: Diagonal Pattern with Larger Storm

In this case, the second storm pattern is used in which the storm starts centered at node 12 and moves along the principal diagonal to reach node 0, but the ellipse parameters are changed. The bigger ellipse has a larger major-axis diameter of 30 km and minor axis diameter of 20 km. The inner ellipses each have major-axis

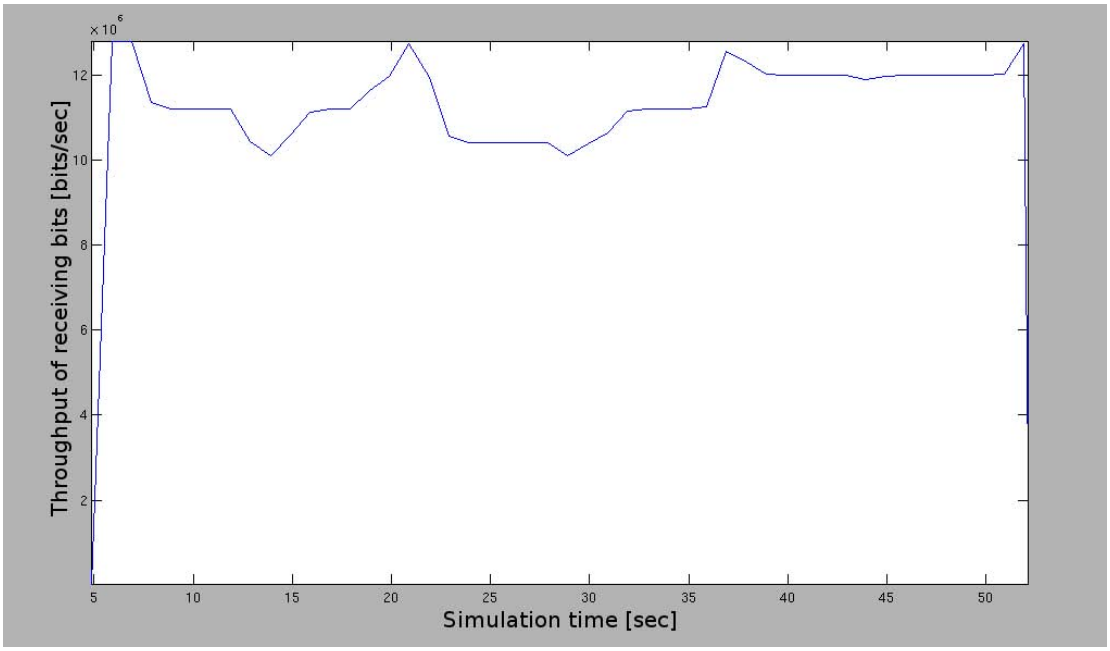

Figure 4.7. Case 2: Throughput of all received bits

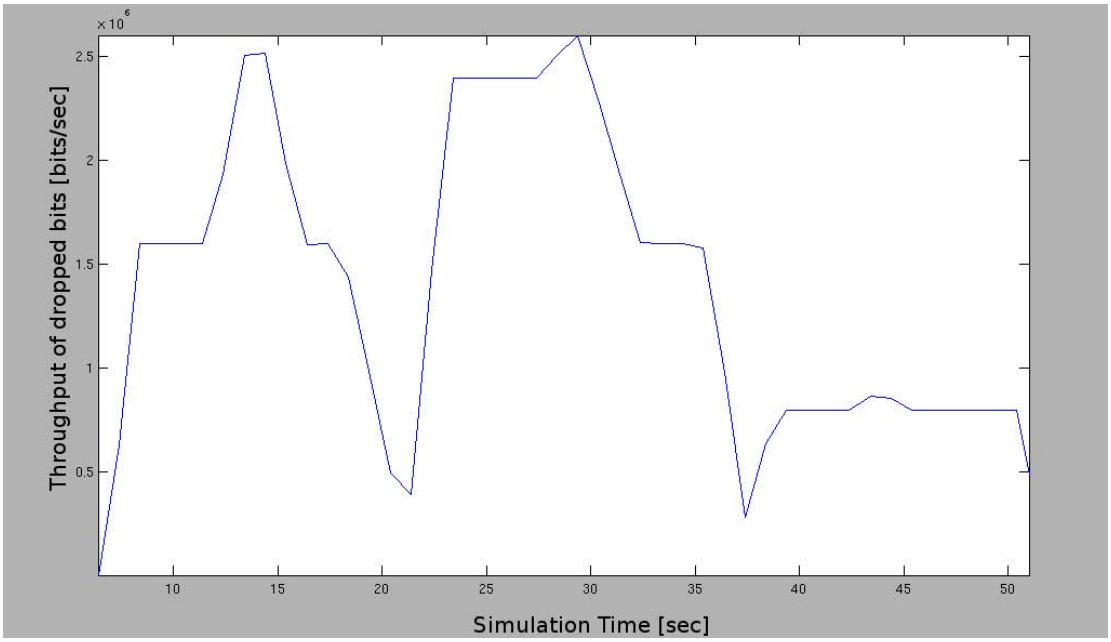

Figure 4.8. Case 2: Throughput of all dropped bits

diameters of nine km and minor axis diameters of five km. Figure 4.9 shows the movement of this storm across the 4×4 mesh. As the storm covers more links at

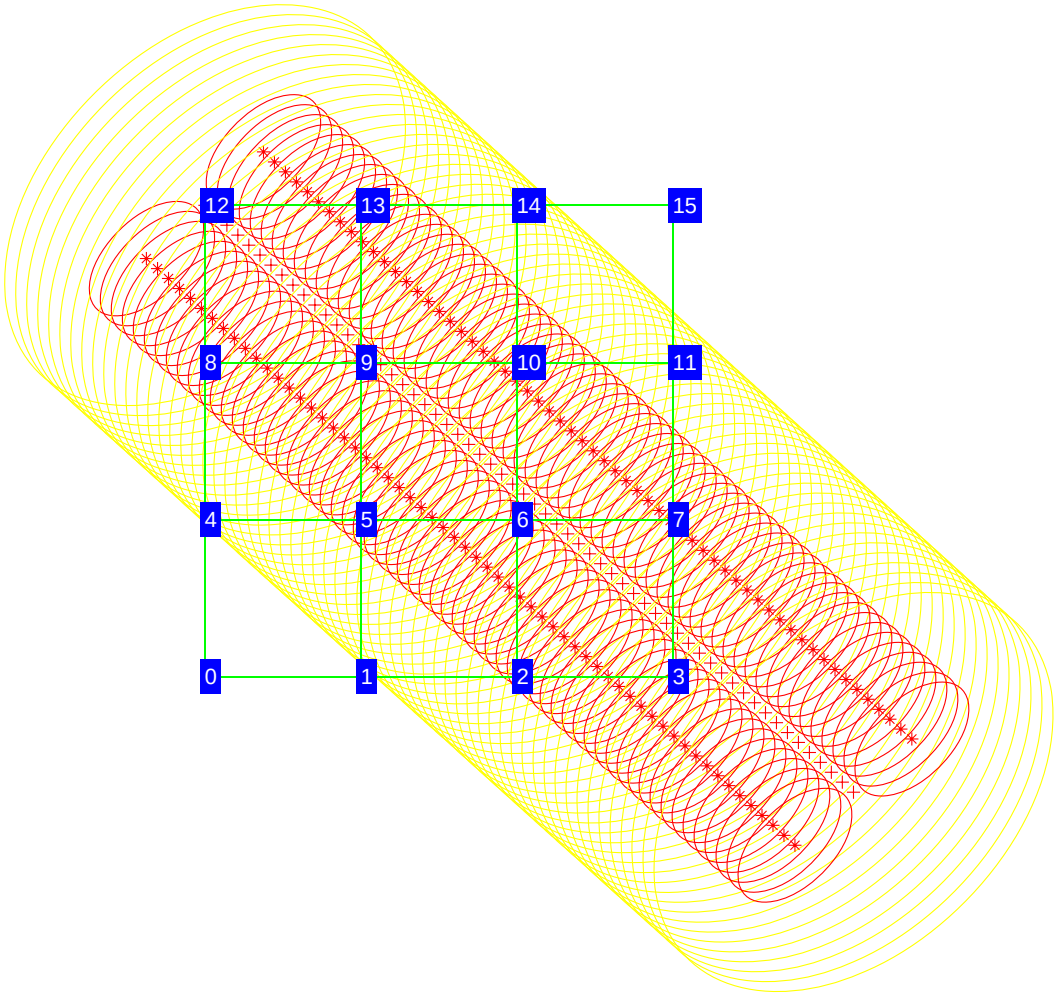

Figure 4.9. Case 3: Storm moves diagonally across the network

each time instant as it passes through, carried load is expected to be lower than the one obtained for Case 2.

Table 4.3 shows the simulation information for the third case where N_s = 154,655 and N_d = 38,079, resulting in a carried load value of $\eta = 75.37\%$ which is worse than Cases 1 and 2. Bigger storms affect more links at the same time, thereby drastically decreasing throughput.

Figure 4.10 shows the throughput of all the received bits in the mesh network.

Table 4.3. Case 3: Simulation information

Simulation length in seconds:	53.19715
Number of nodes:	16
Number of sending nodes:	16
Number of receiving nodes:	16
Number of generated packets:	170240
Number of sent packets:	154655
Number of forwarded packets:	259841
Number of dropped packets:	38079
Number of lost packets:	22494
Minimal packet size:	500
Maximal packet size:	500
Average packet size:	500
Number of sent bytes:	77327500
Number of forwarded bytes:	129920500
Number of dropped bytes:	19039500
Packets dropping nodes:	1 2 4 5 6 8 9 10 12 13

The average throughput is 8.76 Mbps compared to the ideal case of 12.8 Mbps. Figure 4.11 shows the throughput of all the dropped bits for Case 3.

It is seen that even mild rain rates of two mm/h and heavier rain rates of 10 mm/h cause a 10% drop in throughput. Bigger and more intense storms can deteriorate links to the extent of causing complete link outage.

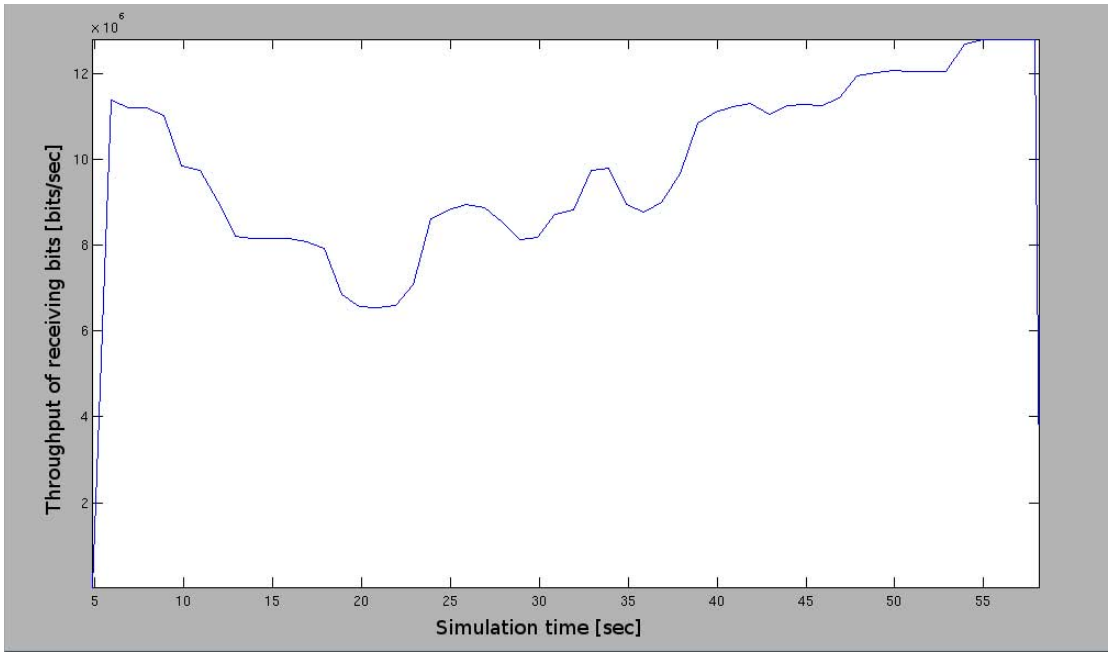

Figure 4.10. Case 3: Throughput of all received bits

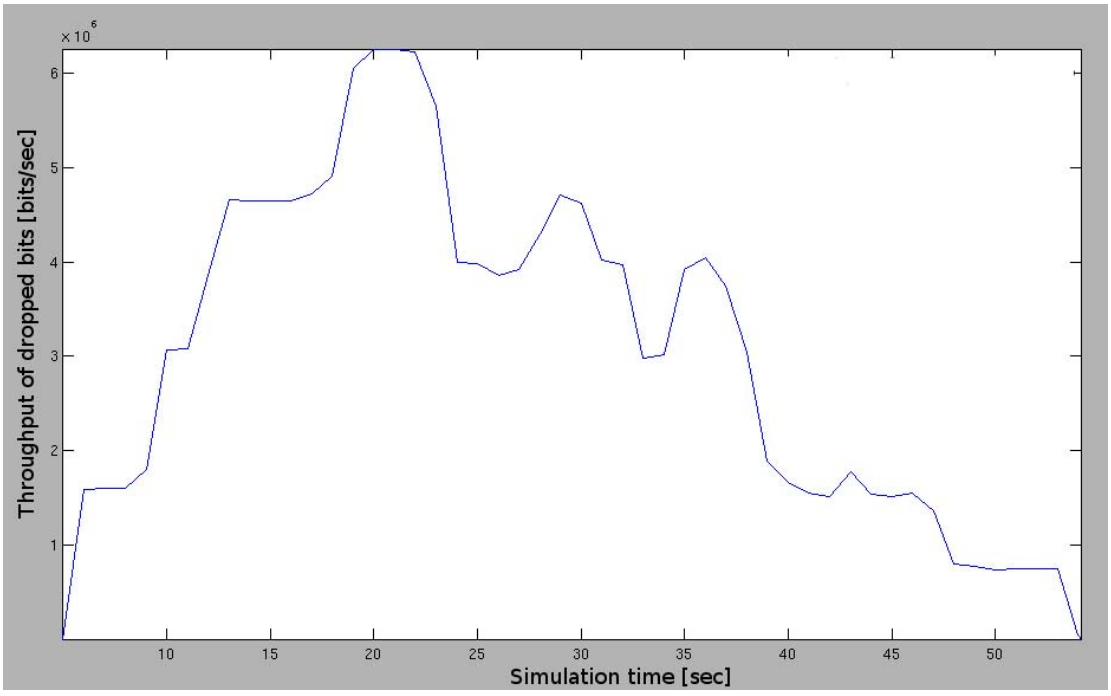

Figure 4.11. Case 3: Throughput of all dropped bits

Chapter 5

Link Modeling

Long-term statistics of rain attenuation are useful for planning link budgets and determining the automatic gain control (AGC) in MWB transceivers [35, 36]. Links are often designed with a knowledge of rain-rate statistics by performing a rain-rate time-series to attenuation time-series conversion [28]. But, when a test link is available, the approximation from rain rate to attenuation becomes needless. A model can be constructed with attenuation measurements obtained directly from the transceivers on the link. In this thesis, one such model is presented.

We propose a three-state Markov model of a link based on FER measurements. The three states, *strong*, *weak* and *disconnected*, each represent a particular range of values of FER. Measured values of FER are categorized into *strongly connected*, *weakly connected* or *disconnected*, based on the thresholds set for each state. A Markov model is then formulated, either for a specific time period such as a stormy day, or for the lifetime of the link. This is discussed in detail in Section 5.3.

This chapter is organized as follows: Markov processes are explained in Section 5.1, the measurement setup is explained in Section 5.2, and the three-state

model is presented in Section 5.3.

5.1 Markov Process

A Markov process is a particular type of stochastic process in which knowledge of the present state is necessary and sufficient to describe the future state. In other words, the future states are independent of the past states and are dependent only on the present state, referred to as memoryless.

Each state represents a random variable $X_i = \{X_1, X_2, X_3 \ldots X_n\}$ where n denotes the number of states and $X_i \ldots X_n$ are random variables with the following property:

$$P\{X_i = x/X_{i-1} \ldots X_1\} = P\{X_i = x/X_{i-1}\} \qquad 1 \leq i \leq n \tag{5.1}$$

The probability of the system to be in a particular state is the *state probability*, and the probability of the system to go from one state to another is the *state-transition probability*. Markov processes are widely used in a variety of applications including building models for weather prediction. In this case, a simple two-state link is considered where the states are *strong* and *disconnected*. The transition probability matrix (TPM) for the two-state link is:

$$P = \begin{bmatrix} p_{11} & p_{12} \\ p_{21} & p_{22} \end{bmatrix} = \begin{bmatrix} 0.7 & 0.3 \\ 0.6 & 0.4 \end{bmatrix} \tag{5.2}$$

where, p_{11} is the probability that the current state of the link is *strong* given it was *strong* in the previous time instant, p_{12} is the probability that the current state of the link is *weak* given it was *strong* in the previous time instant, p_{21} is

the probability that the current state of the link is *strong* given it was *weak* in the previous time instant, and p_{22} is the probability that the current state of the link is *weak* given it was *weak* in the previous time instant. The following is a very important property of the TPM:

$$\sum_{j=1}^{n} p_{ij} = 1 \qquad \forall \quad i \quad \in \quad \{1....n\} \tag{5.3}$$

5.2 Measurement Setup

A two-hop path operating at 73.5 and 83.5 Ghz has been deployed in Lawrence, Kansas. There are four antennas as shown in Figure 5.1. All the antennas have sufficient clearance from the ground, foliage and other interfering structures to permit unobstructed line of sight. The transceivers between the transmitter and receiver are connected back-to-back and the transceiver at the receiving end is looped back to transmit what it receives.

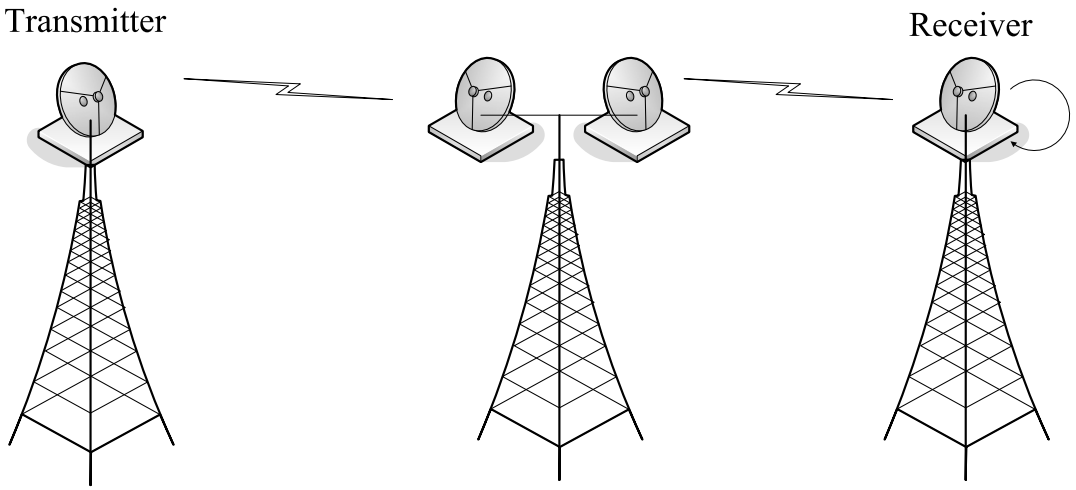

Figure 5.1. MWB test topology

A gigabit ethernet (GigE) tester is connected to the source antenna and trans-

mits 512-byte packets in 30-second intervals at roughly one Gb/s. The GigE tester records parameters such as number of transmitted packets, number of dropped packets, latency, and standard deviation of the latency. FER (frame error ratio) is calculated from the knowledge of transmitted and dropped packets and the link is categorized into the *strong/weak/disconnected* states based on certain threshold values for every time interval. If N_s is the number of packets sent and N_d is the number of packets dropped, then FER is given by:

$$\text{FER} = \left(\frac{N_d}{N_s}\right) \tag{5.4}$$

and the thresholds are defined as follows:

- strongly connected if FER $< T_s$
- weakly connected if $T_s \leq$ FER $\leq T_d$
- disconnected if FER $> T_d$

where T_s is the threshold for strongly connected and T_d is the threshold for disconnected.

From this, a Markov model is constructed and state and state-transition probabilities are calculated. These numbers can be calculated on any time frame of choice. The most useful ones include monthly figures for analyzing worst-month statistics and days that had significant rainfall, both of which help in planning link budgets for a particular geographical area, as weather phenomena are local in nature.

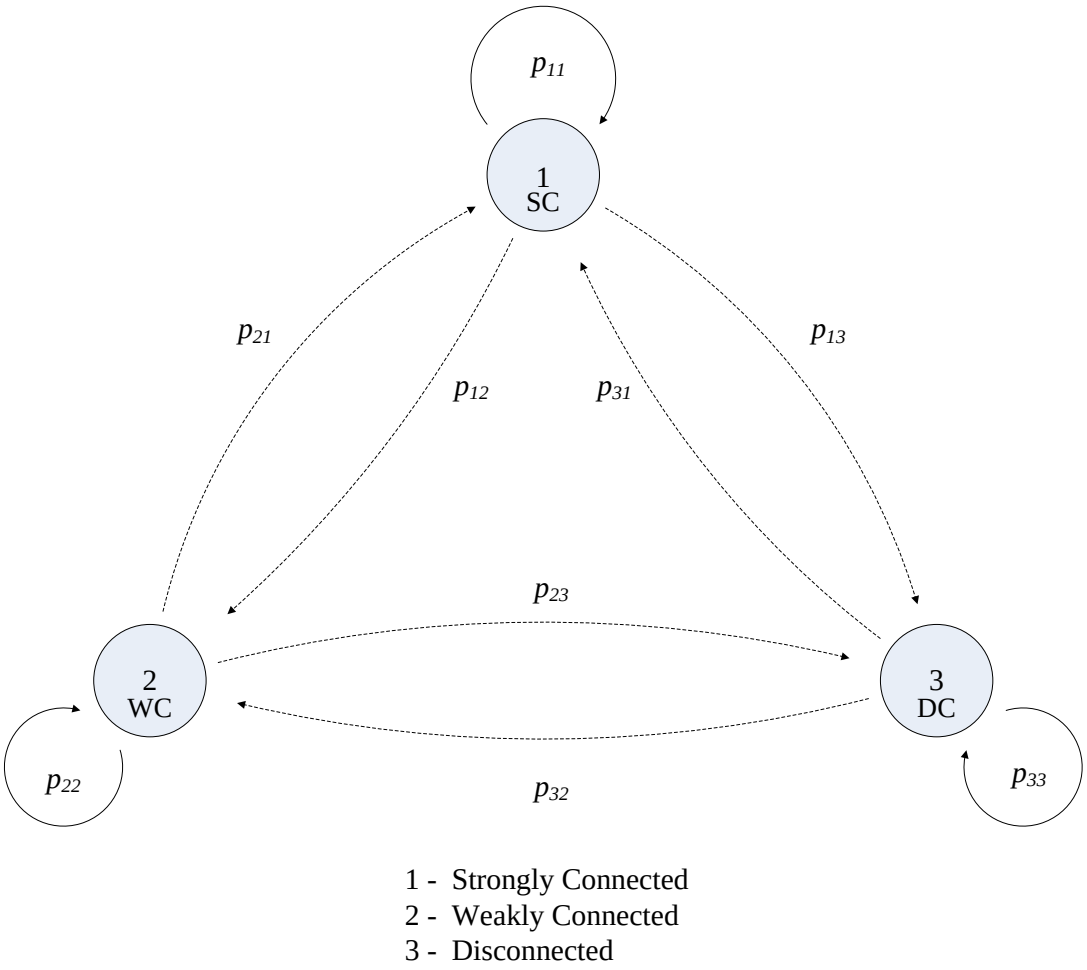

Figure 5.2. Three-state Markov model of link states

5.3 Three-State Markov Model

If we quantize the performance of the link to three states: *strong*, *weak*, and *disconnected*, then the Markov model in Figure 5.2 represents the system. States one, two, and three correspond to the states *strong*, *weak*, and *disconnected* respectively and p_{ij} represents the transition probability from state i to state j and is defined as:

$$p_{ij} = P\{X_{t+1} = j / X_t = i\} \tag{5.5}$$

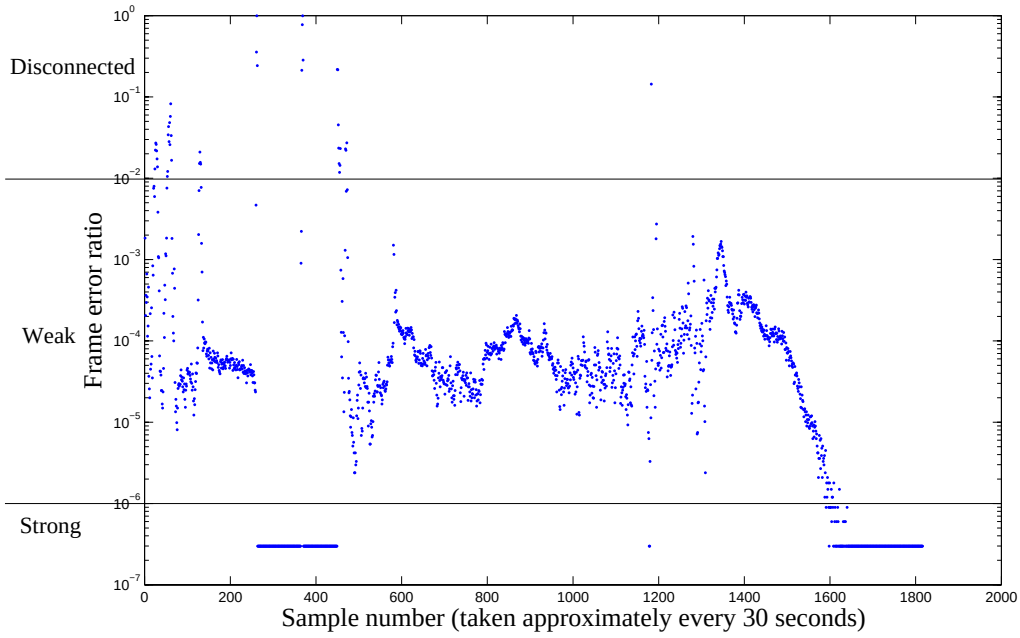

Figure 5.3. Quantization of link performance to three levels

where X is the random variable used to represent the state of the link and $i, j \in \{1, 2, 3\}$. For example, for the case shown in Figure 5.3, the thresholds set are:

- strongly connected if FER $< 10^{-6}$
- weakly connected if $10^{-6} \leq$ FER $\leq 10^{-2}$
- disconnected if FER $> 10^{-2}$

Table 5.1 shows the state probabilities for the *strong*, *weak*, and *disconnected* states and Table 5.2 shows the transition probabilities between the three states for FER measured over a rainy 24-hour period in June 2007. The thresholds used to calculate the probability values are specified. It is seen that changing the thresholds changes the transition probability values. If the availability required is

Table 5.1. 24-hour state probabilities without FEC (Jun. 2007)

State	**Probability**
Strong	0.2159
Weak	0.7614
Disconnected	0.0225

Table 5.2. 24-hour TPM without FEC (Jun. 2007)

State	Strong	Weak	Disconnected
Strong	0.9846	0.0127	0.0025
Weak	0.0036	0.9905	0.0057
Disconnected	0.0487	0.1707	0.7804

high, stricter bounds for strong, weak, and disconnected states can be established. These probability values will then show how long the link stays in a particular state and how often it transitions into other states. In the past, monthly and yearly statistics were typically used in formulating link budgets. But from the measurement results, it is seen that the availability requirements are not met (For carrier grade, it is usually 99.9% to 99.999% or higher.). In this case, the statistics of a rainy day may be very important to meet availability requirements.

Table 5.3. State probabilities with FEC (Jul. 2007–Feb. 2008)

State	**Probability**
Strong	0.9469
Weak	0.0255
Disconnected	0.0275

Table 5.4. TPM with FEC (Jul. 2007–Feb. 2008)

State	Strong	Weak	Disconnected
Strong	0.9869	0.0124	0.0005
Weak	0.4666	0.4965	0.0368
Disconnected	0.0162	0.0383	0.9454

Table 5.3 and Table 5.4 show the state probabilities and state-transition probabilities for FER measurements made on a set of transceivers with forward error correction (FEC) between July 2007 and February 2008. Table 5.5 and Table 5.6 show the state and state-transition probabilities for FER measured on transceivers without FEC over the same time period. It is seen that the strong state probability is much higher with FEC. The transceivers with FEC use a Reed Solomon 204/188 FEC. In both cases, the links do not perform ARQ (automatic repeat request); this is the current practice in commercial MWB equipment.

Table 5.5. State probabilities without FEC (Jul. 2007–Feb. 2008)

State	Probability
Strong	0.3864
Weak	0.5303
Disconnected	0.0833

Table 5.6. TPM without FEC (Jul. 2007 – Feb. 2008)

State	Strong	Weak	Disconnected
Strong	0.9364	0.0633	0.0003
Weak	0.0461	0.9490	0.0049
Disconnected	0.0015	0.0310	0.9675

Steady state values of models like the one described here can be used to generate rain-attenuation time-series [28, 37, 38]. Simulation of rain-rate time-series from the state and state-transition probabilities depends on the duration of attenuation measurement. To simulate isolated rain events or stormy days, the values in Tables 5.1 and 5.2 can be used. In the past, if statistics were required for planning link budgets, worst-month statistics or measurements taken over a longer duration were used. In this case, data is available over eight months, which is used to reasonably predict the availability of the link. These models can be trained by including more data in the calculations. In general, the availability of a link is better when the entire year is taken into account compared to rainy months, but that is not useful in designing links that meet availability requirements. Designing a link with the availability numbers obtained from yearly statistics might cause complete outage of the link during the rainy months. Therefore, the month in which availability is the worst is chosen and the links and network are planned accordingly. Using maximum transmit power, gain of the antennas, and narrow band signals does not help because the network is made of multiple links and all these will lead to interference. The transmission parameters of the transceivers are changed in some cases and in others, multi-hop paths are used instead of one long link. Multi-hop paths may not be an efficient solution always because of cost factors.

The *weak* and *disconnected* state probabilities can help adjust design parameters to increase the availability of the link and the network. If a link is in the *weak* state for a significant portion of the time (50% in the transceivers without FEC), changing design parameters might result in better availability results. It should be noted that all design decisions must comply with the criteria specified

by the FCC presented in Section 2.1.1.

The availability of the transceivers with FEC is ∼94% whereas that of the transceivers without FEC is ∼38%. Though their specifications are different (The transceivers without FEC use two-foot diameter antennas and the ones with FEC use one-foot diameter antennas and they operate at frequencies one GHz apart.), the comparison is not unfair because they are commercial equipment with similar availability specifications. The availability calculated from FER measurements is significantly different. One of the major causes of this, apart from rain, might be the fact that the transceiver without FEC has a two-foot diameter antenna and a beamwidth of 0.6° and therefore will be affected more by error-angle fading and signal loss due to tower sway. Adding Reed-Solomon 204/188 FEC on this transceiver might make the comparison fairer.

Chapter 6

Conclusions and Future Work

Attenuation due to rain is a serious issue in MWB links. If a metropolitan mesh network or a backhaul network is built using MWB links, weather effects have to be considered while planning the link budget as they significantly impact availability figures. Long-term statistics help plan link budgets, but are hardly useful on an event-by-event basis. In the event of rain, network throughput and carried load can be severely affected as shown in Chapter 4. Knowledge of the spatio-temporal effects of rain on the links in a mesh network is required to calculate throughput and efficiency reduction or to implement intelligent routing schemes. This thesis work has presented a method to model the spatio-temporal effects of rain on a mesh network and evaluate network performance in the event of rain and other atmospheric impairments.

To reiterate, the contributions of this research work are:

- Developed a synthetic storm model with structure and trajectory, which represents the characteristics of a real-world storm, and modeled the effects of the storm on an MWB mesh network.

- Simulated the effects of rain attenuation on network performance using ns-2.
- Formulated long-term statistics of rain attenuation using a three-state Markov model. The model is built from actual measurements of frame error rates on a physical link.

In this chapter, conclusions inferred from this work and future enhancements that will improve this work are presented.

6.1 Conclusions

The mass deployment of MWB links depends a lot on our understanding of the effects of atmospheric impairments such as rain on MWB transmissions. Though empirical models prove satisfactory for initial assesment, they are not sufficient for network planning and link budgeting.

This work provides a means of incorporating spatio-temporal effects of rain in a MWB mesh network and a mathematical model derived from actual measurements that provides long-term statistics of the MWB link.

It is seen that approximating the structure of storm cells to ellipses and associating a rain rate to each ellipse according to the intensity of the cell, provides a reasonable method of calculating attenuation across multiple links in a mesh network during a rain event. The movement of the rain cells is also captured, which ensures that each link captures different rain rates at different times, similar to a real life scenario.

The ns-2 simulations prove that a rain event with typical intensity can lead to link outage, therefore, static routing is not sufficient to meet the required availability and reliability standards. Dynamic routing or predictive routing schemes

must be employed if availability in excess of 99% is desired.

The state probability matrices obtained from measurements show that the link is weak for a significant fraction of time. It is possible to move the link to the strong state by modifying parameters such as bandwidth of the link, transmit power, gain of the transmitting and receiving antennas, and modulation schemes. From the state-transition probability matrices, it is seen that it is not unlikely for the link to transition between extreme states.

6.2 Future Work

The basic premise of this research work is that storm cells are elliptical in nature with the smaller ellipses non overlapping and completely contained within the bigger ellipse.

The trajectory of the storm is the locus of the center of the system. The cells move relative to the center of the system and do not have trajectories of their own. This is not the case in real life as the cells and their front typically have different trajectories.

The storm is modeled as one big ellipse with several smaller ellipses contained within it. It is possible to have storm systems with more than one big ellipse.

The ITU model relating attenuation and rain rate is used in this work. Instead, a relationship curve can be plotted with the results of measurements of rain and FER on the physical link setup. From the curve, a table lookup can be done to give a particular value of attenution/FER for a given value of rain rate that is readily available from radar data and rain gauges. This would be more accurate than the ITU model for the region in which the measurements are made. But measurements over a long period of time and a wide range of rain-rate values would be required

to do this. Figure 6.1 shows a preliminary plot of FER measured and derived from the ITU-R P.838-3 recommendation.

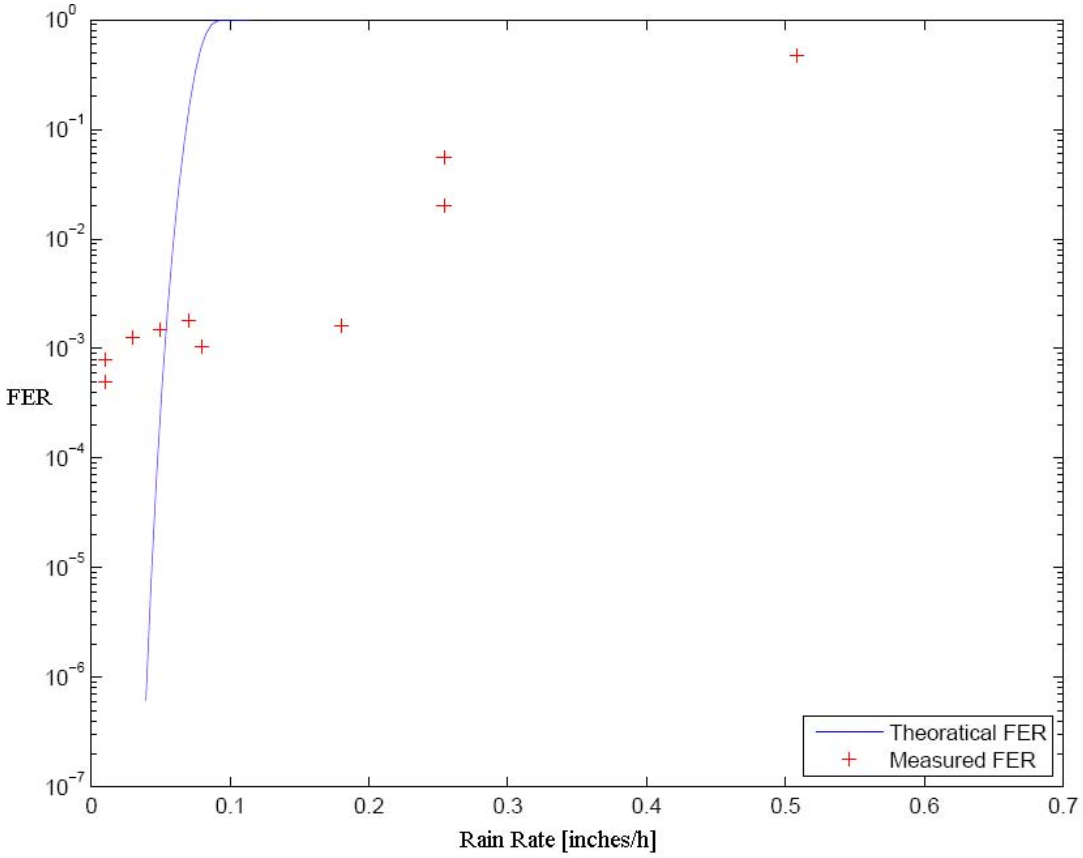

Figure 6.1. Measured FER vs. FER derived from ITU-R P. 838-3

All nodes in the network are set to transmit and receive at the same frequency. Though this assumption is reasonable considering the properties of MWB transmissions in the real world, transceivers will operate at different bands within the MWB. For more accurate results, this must be considered.

In a mesh network operating at MWB, intelligent routing schemes could be devised to circumvent the problems caused by rain attenuation and make efficient use of the links in the network. Exploring different routing schemes to find optimal

solutions is an excellent problem that needs to be addressed.

The Markov model built to measure long-term probabilities of attenuation uses 3 states: *strong*, *weak*, and *disconnected*. The number of states can be increased and the thresholds can be modified to obtain better resolution if needed.

Appendix A

ITU-R P.838-3 Coefficients

Table A.1. Coefficients for k_H

j	a_j	b_j	c_j	m_k	c_k
1	-5.33980	-0.10008	1.13098	-0.18961	0.71147
2	-0.35351	1.26970	0.45400		
3	-0.23789	0.86036	0.15354		
4	-0.94158	0.64552	0.16817		

Table A.2. Coefficients for k_V

j	a_j	b_j	c_j	m_k	c_k
1	-3.80595	0.56934	0.81061	-0.16398	0.63297
2	3.44965	-0.22911	0.51059		
3	-0.39902	0.73042	0.11899		
4	0.50167	1.07319	0.27195		

Table A.3. Coefficients for α_H

j	a_j	b_j	c_j	m_α	c_α
1	-0.14318	1.82442	-0.55187	0.67849	-1.95537
2	0.29591	0.77564	0.19822		
3	0.32177	0.63773	0.13164		
4	-5.37610	-0.96230	1.47828		
5	16.1721	-3.29980	3.43990		

Table A.4. Coefficients for α_V

j	a_j	b_j	c_j	m_α	c_α
1	-0.07771	2.33840	-0.76284	-0.053739	0.83433
2	0.56727	0.95545	0.54039		
3	-0.20238	1.14520	0.26809		
4	-48.2991	0.791669	0.116226		
5	48.5833	0.791459	0.116479		

References

[1] GigaBeam Corporation. New Spectrum Bands Enable GigaBeam's WiFiber Revolution. [Online]. Available: http://www.gigabeam.com/technology.cfm

[2] FCC, "Millimeter Wave Propagation: Spectrum Management Implications," Bulletin Number 70, 1997.

[3] Mike Willis. Absorption by Atmospheric Gases. [Online]. Available: {http://www.mike-willis.com/Tutorial/gases.htm}

[4] W. Myers, "Comparison of Propagation Models," *IEEE P802.16 Broadband Wireless Access Working Group*, 1999. [Online]. Available: {http://www.ieee802.org/16/tg2_orig/contrib/80216cc-99_13.pdf}

[5] Cisco Systems Inc. (May 16,2003) 02-146 ExParte FCC WTB. [Online]. Available: {http://www.gigabeam.com/FCC_Information/Cisco_FCC_ExParte_Filing_May_16_2003.pdf}

[6] D. Lockie, "Upper Millimeter-wave History, Technology and Applications for Gigabit Class Communications Service," IEEE 802 LMSC Plenary Session, 2002. [Online]. Available: {http://www.ieee802.org/802_tutorials/march02/T80216-02_02b.pdf}

[7] Information Sciences Institute, "NS-2 Network Simulator," Software Package, 2003. [Online]. Available: {http://www.isi.edu/nsnam/ns/}

[8] "Allocations and Service Rules for the 71-76 GHz, 81-86 GHz and 92-95 GHz Bands," Memorandum and Opinion Order (FCC 03–248), 2003.

[9] "Allocations and Service Rules for the 71-76 GHz, 81-86 GHz and 92-95 GHz Bands," Memorandum and Opinion Order (FCC 05–45), 2005.

[10] R. A. Nelson. Antennas. [Online]. Available: {http://www.aticourses.com/antennas_tutorial.htm}

[11] T. S. Rappaport, *Wireless Communications: Principles and Practice*. Pearson Education Inc., 2004, pp. 126–128.

[12] Comité Consultatif International pour la Radio, "Propagation in Non-ionized Media," in *Recommendations and Reports of the CCIR, Vol. V*, 1990.

[13] G. Brussard and P. Watson, *Atmospheric Modelling and Millimeter Wave Propagation*. Chapman and Hall, London, 1995.

[14] Y.Yan, "Microwave Propagation in Saline Dust Storms," *International Journal of Infrared and Millimeter Waves*, vol. 25 No. 8, pp. 1337–1243, 2004.

[15] T. Garlington, "Millimeter E-Band Radio," US Army Information Systems Engineering Command, 2006. [Online]. Available: {http://www.hqisec.army.mil/isec/publications/Millimeter_Wave_E-Band_Radio_May06.pdf}

[16] "Effects of Tropospheric Refraction on Radiowave Propagation," in *CCIR Report 718-2*, vol. 5, 1986.

[17] G. S. Feldhake and L. Ailes-Sengers, "Comparison of Multiple Rain Attenuation Models with Three Years of Ka Band Propagation Data Concurrently Taken at Eight Different Locations," *Online Journal of Space Communication*, vol. 2, 2002.

[18] C. E. Mayer and B. E. Jaeger, "Rain Attenuation Model Comparison and Validation," *Online Journal of Space Communication*, vol. 2, 2002.

[19] R. K.Crane, *Electromagnetic Wave Popagation Through Rain.* John Wiley & Sons Inc., 1996, pp. 139–184.

[20] R. K. Crane, "Prediction of Attenuation by Rain," *IEEE Transactions on Communications*, vol. 28, pp. 1717–1733, 1980.

[21] "Specific Attenuation Model for Rain for use in Prediction Methods," *Recommendation ITU-R P.838-3*, 1992–1999–2003–2005.

[22] Bridgewave Communications. Extended-Range Wireless Gigabit Ethernet Link Model GE60X. [Online]. Available: {http://www.commconnect.com/documents/GE60X_Datasheet.pdf}

[23] G. Hendrantoro, Indrabayu, T. Suryani, and A. Mauludiyanto, "A Multivariate Autoregressive Model of Rain Attenuation on Multiple Short Radio Links," *IEEE Antennas and Wireless Propagation Letters*, vol. 5, pp. 54–57, 2006.

[24] A. Dissanayake, J. Allnutt, and F. Haidara, "A Prediction Model that Combines Rain Attenuation and Other Propagation Impairments along Earth-Satellite Paths," *Online Journal of Space Communication*, 2002.

[25] T. Utsunomiya and M. Sekine, "Rain Attenuation at Millimeter and Submillimeter Wavelengths," *International Journal of Infrared and Millimeter Waves*, vol. 26, no. 6, pp. 905–920, 2005.

[26] C. Alasseur, A. Núñez, F. Fontán, L. Husson, U.-C. Fiebig, and P. Mariño, "Two approaches for effective modelling of rain-rate time-series for radiocommunication system simulations," *Space Communications*, vol. 20, no. 1–2, pp. 69–83, 2005.

[27] M. Montopoli, F. S. Marzano, G. Vulpiani1, A. Fornasiero, P. P. Alberoni, L. Ferraris, and N. Rebora, "Spatial Characterization of Raincell Horizontal Profiles from C-band Radar Measurements at Mid-latitude," *Advances in GeoSciences*, vol. 7, pp. 285–292, 2006.

[28] F. Fontan, A.Nunez, A. Valcarce, and U.C.Fiebig, "Converting Simulated Rain-rate Series into Attenuation Series Using the Synthetic Storm Technique," in *3rd International Workshop on Propagation Impairment Mitigation for Millimeter Wave Radio Systems*, 2005.

[29] A.Daru, Z. Kormanyos, and J.Bito, "Space and Time Correlation of Rain Attenuation in Millimeter Wave Feeder Network," in *COST Action 280* 1^{st} *International Workshop*, July 2002.

[30] C. Riva, "Spatial Characteristics of Propagation Parameters: A Review," in *COST Action 280* $1^{s}t$ *International Workshop*, July 2002.

[31] G. C. Pomraning, "Transport Theory in Discrete Stochastic Mixtures," in *Advances in Nuclear Science and Technology*, vol. 24. Springer US, 1996, pp. 47–93.

[32] B. Su and G. C. Pomraning, "A Stochastic Description of a Broken Cloud Field," *Journal of Atmospheric Sciences*, vol. 51, pp. 1969–1977, 1993.

[33] A. Kassler, M. Castro, and P. Dely, "VoIP Packet Aggregation based on Link Quality Metric for Multihop Wireless Mesh Networks," in *Cost 290 6th MCM*, 2007.

[34] J. Postel, "User Datagram Protocol," in *RFC 768*, 1980.

[35] M. R. Islam, "Frequency Scaling Technique for Rain Attenuation Prediction on Terrestrial Microwave Links in Tropical Climate," in *ICECE 2002*, December,2002, pp. 372–375.

[36] K. S. Paulson and J. W. F. Goddard, "Report on Link Reliability Project: Winchester and Thorne Hill," Project Report D36-5, July,2002. [Online]. Available: http://www.ofcom.org.uk/static/archive/ra/topics/research/rcru/project36/WinchThornD36-5.pdf

[37] M. van de Kamp, "Rain Attenuation as a Markov Process: The Meaning of Two Samples," in *COST Action 280 1^{s}t International Workshop*, July 2002.

[38] P. Hou, J. Zhuang, and G. Zhang, "A Rain Fading Simulation Model for Broadband Wireless Access Channels in Millimeter Wavebands," *51st Vehicular Technology Conference*, pp. 2559–2563, 2000.